Karlsruhe Institute of Technology

Annual Report 2019

Institute for Pulsed Power and Microwave Technology
Institut für Hochleistungsimpuls- und Mikrowellentechnik

John Jelonnek (ed)

Annual Report 2019

Institute for Pulsed Power and Microwave Technology
Institut für Hochleistungsimpuls- und Mikrowellentechnik

John Jelonnek (ed)

Part of this work was supported by ITER Organization under the task agreement C52TD53FE. The views and opinions expressed herein reflect only the authors views. The ITER Organization is not liable for any use that may be made of the information contained therein.

Part of this work has been carried out within the framework of the EUROfusion Consortium and has received funding from the Euratom research and training programme 2014-2018 and 2019- 2020 under grant agreement No. 633053. The views and opinions expressed herein do not necessarily reflect those of the European Commission. Parts of the simulations presented in this work have been carried out using the HELIOS supercomputer at IFERC-CSC.

Part of this work is supported by Fusion for Energy (F4E) under Grants F4E-GRT-553 and within the European GYrotron Consortium (EGYC). EGYC is a collaboration among SPC, Switzerland; KIT, Germany; HELLAS, Greece; IFP-CNR, Italy. The views expressed in this publication do not necessarily reflect the views of the European Commission.

Impressum

Karlsruher Institut für Technologie (KIT)

KIT – Die Forschungsuniversität in der Helmholtz-Gemeinschaft

Institute for Pulsed Power and Microwave Technology (IHM)

Institut für Hochleistungsimpuls- und Mikrowellentechnik (IHM)

Director: Prof. Dr.-Ing. John Jelonnek

The Institute for Pulsed Power and Microwave Technology (Institut für Hochleistungsimpuls- und Mikrowellentechnik (IHM)) is doing research in the areas of pulsed power and high-power microwave technologies. Both, research and development of high power sources as well as related applications are in the focus. Applications for pulsed power technologies are ranging from materials processing to bioelectrics. High power microwave technologies are focusing on RF sources (gyrotrons) for electron cyclotron resonance heating of magnetically confined plasmas and on applications for materials processing at microwave frequencies.

The IHM is doing research, development, academic education, and, in collaboration with the KIT Division IMA and industrial partners, the technology transfer. The IHM is focusing on the long term research goals of the German Helmholtz Association (HGF). During the ongoing program oriented research period (POF3) of HGF (2015 – 2020), IHM is working in the research field ENERGY. Research projects are running within following four HGF programs: “Energy Efficiency, Materials and Resources (EMR)”; “Nuclear Fusion (FUSION)”, “Nuclear Waste Management, Safety and Radiation Research (NUSAFE)” and “Renewable Energies (RE)”.

During 2019, R&D work has been done in the following areas: fundamental theoretical and experimental research on the generation of intense electron beams, strong electromagnetic fields and their interaction with biomass, materials and plasmas; application of those methods in the areas of energy production through controlled thermonuclear fusion in magnetically confined plasmas, in material processing and in energy technology.

Mentioned long-term research areas require the profound knowledge on modern electron beam optics, high power micro- and millimeter waves, sub-THz technologies, vacuum electronics, material technologies, high voltage technologies and high voltage measurement techniques.

Table of Contents

1 Nuclear Fusion (FUSION): Plasma Heating Systems -Microwave Plasma Heating & Current Drive Systems-

Contact: Dr. Gerd Gantenbein

The Department for High Power Microwave Technologies focuses on the research and development of high power RF sources (gyrotrons) and related components for electron cyclotron resonance heating and current drive (ECRH&CD) of magnetically confined nuclear fusion plasmas. Additionally, it is involved in research and development in the field of and on the application of microwaves to chemical processes, materials and composites.

In particular the following major activities have been carried out in 2019:

- Gyrotron development for W7-X, targeting at 1.5 MW RF power at 140 GHz, numerical simulations and manufacturing of components for a short pulse pre-prototype tube.
- Experimental study on further performance optimization of the European 1 MW, 170 GHz hollow-cavity gyrotron prototype for ITER, investigations on advanced beam tunnels.
- 2 MW, 170 GHz longer-pulse coaxial-cavity gyrotron prototype, upgrade of the modular short pulse gyrotron with internal cooling systems, demonstration of increased pulse length of up to 50 ms.
- Gyrotron development for DEMO, with the focus on increasing the operation frequency in a first step to 204 GHz and efficiency enhancement by multi-staged depressed collectors, low power excitation of $TE_{40,23}$ mode at 203.92 GHz and manufacturing of a first 3-D model of a MSDC.
- Code developments in numerical codes to include ohmic losses in the design of mirrors and waveguide components using KarLESSS package.
- Investigation on a broadband polarizer mitre bend in the frequency range from 90 to 100 GHz.
- FULGOR: Progress in the construction of the new gyrotron test stand, procurement and installation diagnostic systems.
- First experimental tests of a diagnostic tool to characterize magnetron injection guns for fusion gyrotrons.
- Development of a new feedback system for a passive mode locked pulsed oscillator operating at 263 GHz in the frame of generation of ultra-short pulses with new gyro-devices.

1.1 Gyrotron Development for W7-X

Contact: Dr. Konstantinos Avramidis

In November 2018, the Scientific Board (Wissenschaftlichen Leitung) of IPP decided to proceed with the upgrade of the W7-X ECRH system, taking into account the request for higher EC power as well as the feasibility of the upgrade, assessed by IPP and KIT/IHM. For this upgrade, the development of a Continuous-Wave (CW) 1.5 MW, 140 GHz prototype gyrotron has started and the contract between IPP and the industrial partner (Thales, Vélizy-Villacoublay, France) was signed in 2019. KIT/IHM is involved in the development within the framework of EUROfusion Work Package Stellarator 1 (WPS1). In particular, KIT/IHM has undertaken the scientific design of the 1.5 MW tube with contributions from IPP and NCSRD/NKUA. The scientific design has been completed and forwarded to the industrial partner. It incorporates the Magnetron Injection Gun (MIG), the beam tunnel, the cavity and non-linear uptaper, and the quasi-optical system (launcher and three mirrors). A Final Design Review Meeting is scheduled for autumn 2020 and the CW tube delivery is foreseen for mid 2021. The design for the 1.5 MW gyrotron is an upgrade of the successful design of the existing 1 MW, 140 GHz gyrotrons at W7-X, combining risk mitigation and cost control. Significant improvements are incorporated, including a larger cavity, improved cooling, improved beam tunnel, and an adjustable 3rd mirror. A typical result from time-dependent simulations of the diode start-up of the cavity is shown in Fig. 1.1.1, where an RF power of 1.6 MW with 38% interaction efficiency is achieved at the operating point of 80 kV / 55 A.

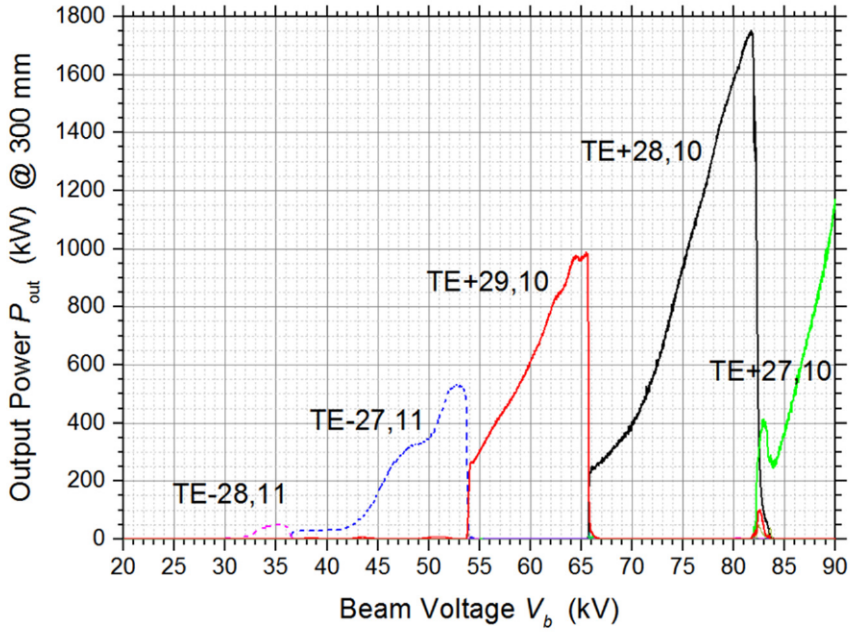

Fig. 1.1.1: Simulated multi-mode start-up (44 competing modes) of the 1.5 MW gyrotron at 55 A current, showing excitation of the operating $TE_{28,10}$ mode at the nominal beam energy (80 keV).

In parallel to the CW prototype development, the development of a short-pulse (ms) 1.5 MW gyrotron has also started, under responsibility of KIT/IHM. The short-pulse gyrotron has an identical scientific design to that of the CW prototype. This gyrotron will support the development of the prototype and mitigate the risks by providing early experimental validation, in short-pulse operation, of the scientific design of all critical components. The engineering drawings for the short-pulse gyrotron and an accompanying XY-table for the tube alignment in the magnet have been completed. Several major components have already been

fabricated, including the mirror box and the quasi-optical system (Fig. 1.1.2), the XY-table, and the parts for the beam tunnel assembly. The MIG has been ordered from Thales. Completion of the fabrication, assembly of the tube, and experimental testing are foreseen for the next period. The fabricated quasi-optical system has been successfully tested in the low power measurement set-up at IHM showing very good performance (Fig. 1.1.2). From the measurements, a vector Gaussian mode content above 97 % for the RF beam at the window position was calculated, which is close to the theoretical predictions.

Currently, for Collective Thomson Scattering (CTS) diagnostics at W7-X, one of the gyrotrons of the ECRH system operating at 140 GHz is used as probing source. A more efficient CTS is possible using a higher frequency at ~175 GHz. Within EUROfusion WPS1, the possibility to operate the existing W7-X ECRH gyrotrons at ~175 GHz was theoretically investigated in detail, focusing on the behaviour of the three related components, namely the electron gun, the cavity, and the quasi-optical system. Nine candidate operating modes for the ~175 GHz operation were studied and the most promising choice appears to be the $TE_{34,10}$ mode, achieving at 173.9 GHz a generated power in the cavity around 650 kW in short-pulse operation and around 550 kW in long-pulse operation. The frequency of 173.9 GHz results in a reflection of the RF beam at the window of 0.84 %, whereas the Gaussian mode content of the RF beam is calculated to be ~87 %. These results indicate that implementing a 175 GHz CTS diagnostic at W7-X using the existing gyrotrons is possible, in principle. Relevant experimental tests on the gyrotron operation at 175 GHz are foreseen as soon as a 7 T magnet is available at W7-X.

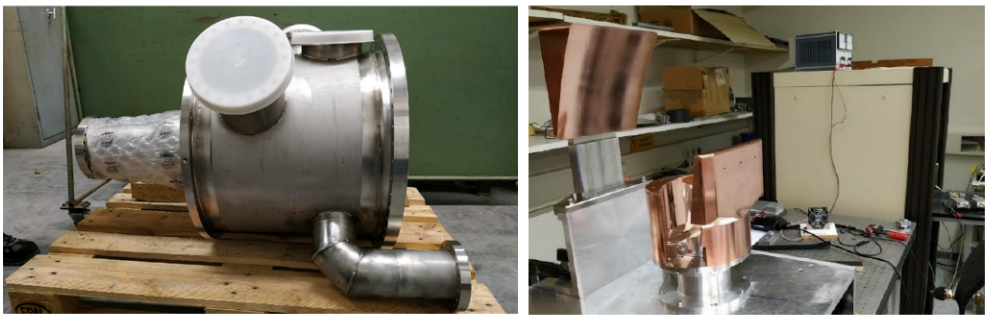

(a) (b)

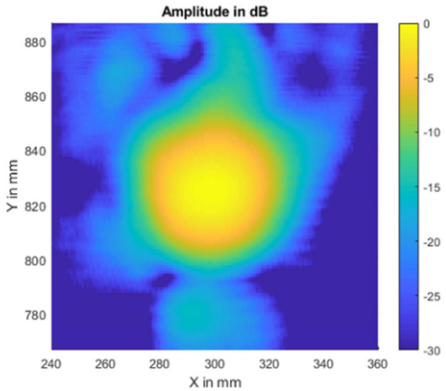

(c)

Fig. 1.1.2: (a): Mirror box of the short-pulse gyrotron. (b): Quasi-optical system of the short-pulse gyrotron (installed in the low-power measurement set-up). (c): Low power measurement of the field pattern after the quasi-optical system, at the position of the gyrotron window.

1.2 Gyrotron Development for ITER

Contact: Dr. Tomasz Rzesnicki

1.2.1 Experimental study on the improved version of the beam tunnel with the short-pulse 1 MW, 170 GHz gyrotron prototype for ITER.

In several of the recent experiments with MW-class gyrotrons, the tubes suffered from parasitic oscillations that were excited in the region of the beam-tunnel. Those parasitic oscillations are a significant threat for the gyrotron operation, since they can reduce the quality of the beam (due to increased spread) before the beam-wave interaction takes place in the cavity. As a result, the RF output power and the efficiency of the gyrotron could be limited, the gyrotron could suffer from increased thermal loads at unpredicted positions which might result in damages and the pulse length could be reduced due to arcing or intense outgassing. Two different solutions for the improvement of the beam tunnel structure have been considered: (1) a simple fully metallic construction with optimized outer wall shape (Fig. 1.2.1) and (2) the typical construction (combination of copper and ceramic rings) with an optimized geometry and improved ceramic material properties (Fig. 1.2.2). The first approach is interesting due to its simplicity and kind of materials (metallic construction) and could be a perfect alternative for the currently existing one, which is more complicated and expensive. The first prototype of a fully metallic structure (Fig. 1.2.3) with an optimized inner wall contour was installed in the 1 MW, 170 GHz gyrotron for verification and was successfully tested experimentally providing very encouraging results. In particular, during the tests in a wide range of operating points, no parasitic signals were observed.

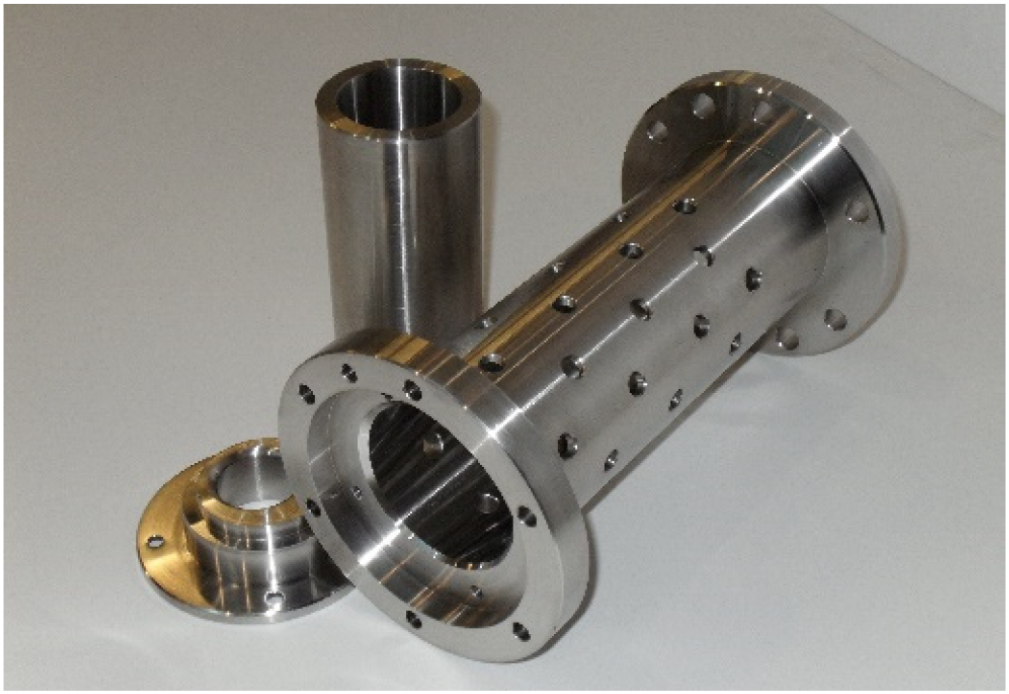

Fig. 1.2.1: First prototype of the fully metallic beam tunnel.

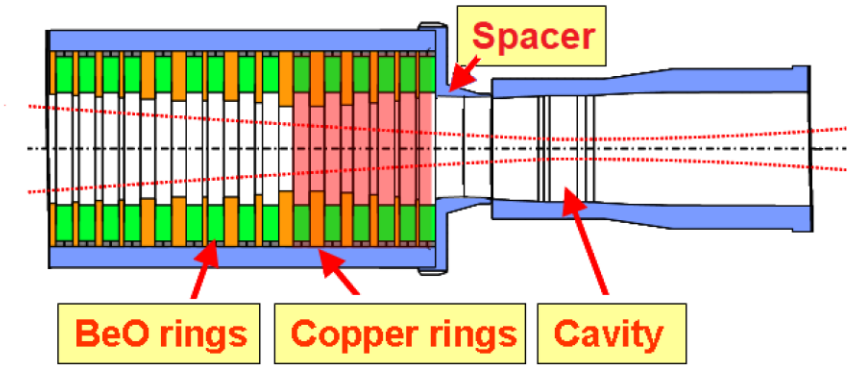

Fig. 1.2.2: Improved version of the loaded beam tunnel.

In order to remain compatible with the existing technology of the CW gyrotron tubes, another approach was to optimize the existing beam tunnel geometry and to replace the currently used ceramic material (BeOSiC) by another one with more appropriate dielectric properties. According to theoretical studies, a significantly lower concentration of the lossy additive to the ceramic is preferable. In brief, by reducing the concentration of SiC, the resulting ceramic has now lower (both real and imaginary part) permittivity. In turn, the potentially generated RF electric field in the beam-tunnel area has the possibility to penetrate deeper into the dumping material, increasing in this way the overall losses. That is not the case for a highly lossy material, which due to the large reflection coefficient on the interface between the vacuum and the dielectric reflects the RF electric field. Such beam tunnel was manufactured using BeOSiC-ceramic rings with a reduced concentration of the SiC and properly modified geometry of the neighboring copper rings and was tested. The experimental results verify the simulations and show that the number of the potential parasitic modes has been significantly reduced, especially for frequencies below 151 GHz. Frequencies above 151 GHz have been considered to be excited in the metallic spacer area (see Fig. 1.2.2), where there are no ceramic rings. Based on this observation, additional experiments are scheduled for 2020, with a modified beam tunnel version in which the damping structure has been extended up to the cavity (replacing the metallic spacer).

1.2.2 Progress in the development of the 2 MW, 170 GHz Longer-Pulse Coaxial-Cavity Gyrotron

A development of a Longer-Pulse (LP) coaxial-cavity gyrotron with the goal of generating 2 MW of RF power at 170 GHz with pulse duration of up to ~100 ms in the first step and up to ~1 s in the second is in progress at IHM. In order to support this goal, multiple upgrades have been performed to the standard Short-Pulse (SP) (with 1 ms pulse length) construction of the gyrotron. First, the key components of the tube have been equipped with cooling systems. Second, a new triode MIG has been manufactured and installed for the tests in the gyrotron. In addition, various modifications have been performed on the gyrotron body in order to address several important issues observed during previous campaigns. First of all, the interface between the mirror-box and the collector was modified towards better vacuum tightness especially during the backing-out process. A commercial HELICOFLEX sealing, which resulted in an excellent vacuum condition in the order of 10^{-10} mbar after the baking-out process is used (see Fig. 1.2.3). Another issue that was observed in the previous experimental campaigns is a relatively high body current, which was partially addressed to reflected secondary electrons from the area of the collector. As a solution, an additional trajectory-correcting coil (Fig. 1.2.4) was installed inside the water-jacket of the collector. In addition, after some adaptation, the double-wall mirror-box was connected to the external cooling system.

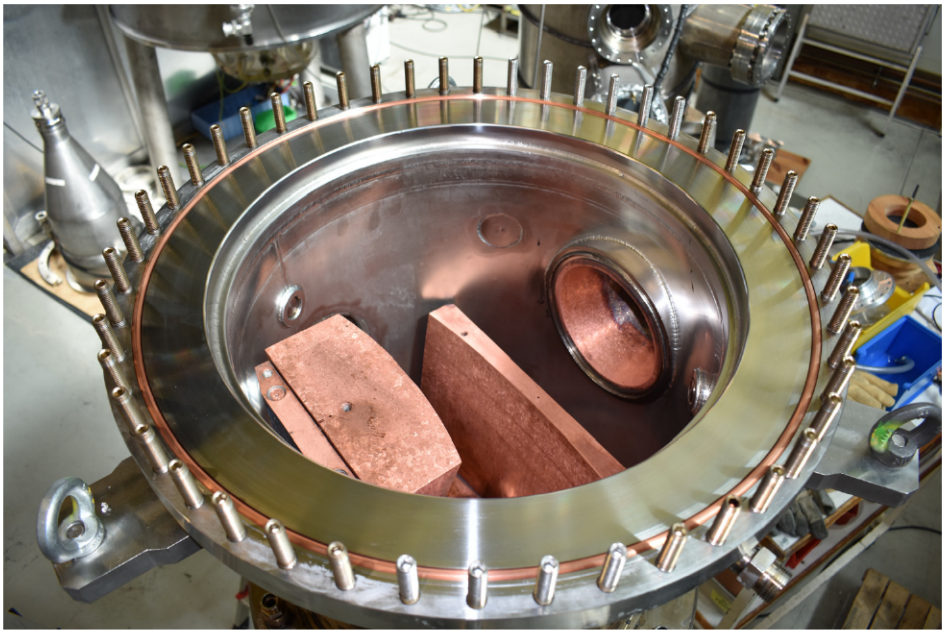

Fig. 1.2.3: Modifications on the mirror-box flange.

After the successful baking-out of the gyrotron, the cathode emitter has been conditioned with a filament current of up to 24 A and the vacuum conditions in the tube were excellent and significantly better than those of the previous experimental set-up. The pulse length extension of this configuration (fused silica window, short-pulse collector, absence of a collector sweeping system) is practically limited to 50 ms. This is a conservative limit in order to minimize mainly the risk of failure of the collector. A second limit on the pulse length is set by the diagnostics and in particular by the short-pulse flow-through calorimeter that is used for the measurement of the generated RF power. Up to end of 2019 it was possible to demonstrate 1 MW with 10 ms pulses, 1.5 MW with 7 ms pulses and 2 MW with 5 ms pulses. Additionally a single pulse of 800 kW with pulse duration 25 ms was also performed successfully. The efficiency of these pulses is close to 45 %, which is very encouraging for achieving the 50 % target after optimizing the operation of the tube. The experiments will be continued in 2020 after replacing the short-pulse flow-through calorimeter with the middle-pulse flow-through calorimeter (LP load).

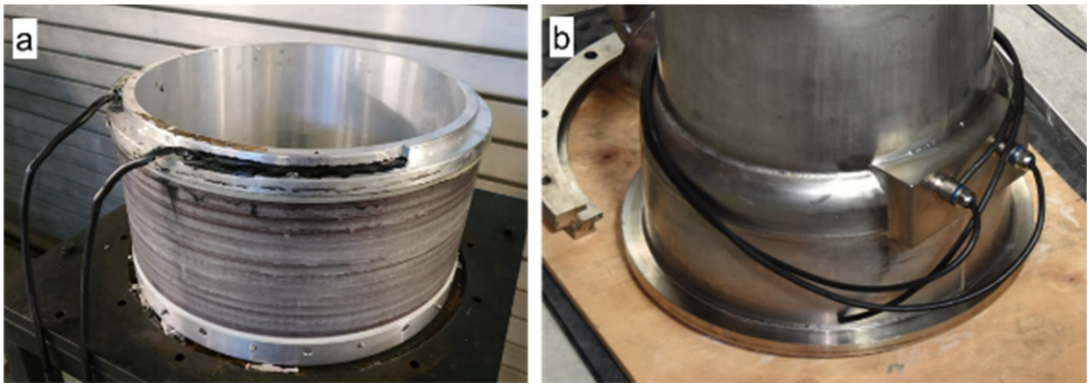

Fig. 1.2.4: Implementation of the trajcetory-correcting coil.

1.3 Gyrotron Development for DEMO

Contact: Dr. Konstantinos Avramidis

The R&D related to the gyrotron for DEMO is in line with the European Fusion Roadmap towards a demonstration power plant and it is performed, at the largest part, within the Work Package Heating and Current Drive (WPHCD) of EUROfusion. The current European DEMO1 baseline poses significant challenges on the gyrotron. These are the need for dual, high-frequency operation (170/204 GHz) and/or fast frequency step-tunability, as well as the requirements for higher power (2 MW), higher overall efficiency (≥ 60 %), and a higher level of reliability and industrialisation, in line with that of a power plant. To keep the gyrotron R&D relevant with respect to possible baseline changes and to alternative reactor configurations towards a future power plant, efficient MW-class gyrotron operation at higher (~240 GHz) frequencies is also considered in parallel.

The advanced concept of the coaxial gyrotron has been selected as being the most promising, compared to the conventional hollow-cavity gyrotron, towards the higher power and frequency targets. The 170 GHz, 2 MW short-pulse coaxial gyrotron at KIT has already exhibited excellent performance at ~1 ms pulses. The next step for coaxial gyrotron technology towards DEMO is to prove experimentally its capability for long-pulse operation. To this end, a first configuration of a longer-pulse 170 GHz, 2 MW coaxial cavity gyrotron has been developed at KIT (for details see 1.2.2). Preliminary results for 5 ms pulse length are shown in Fig. 1.3.1.

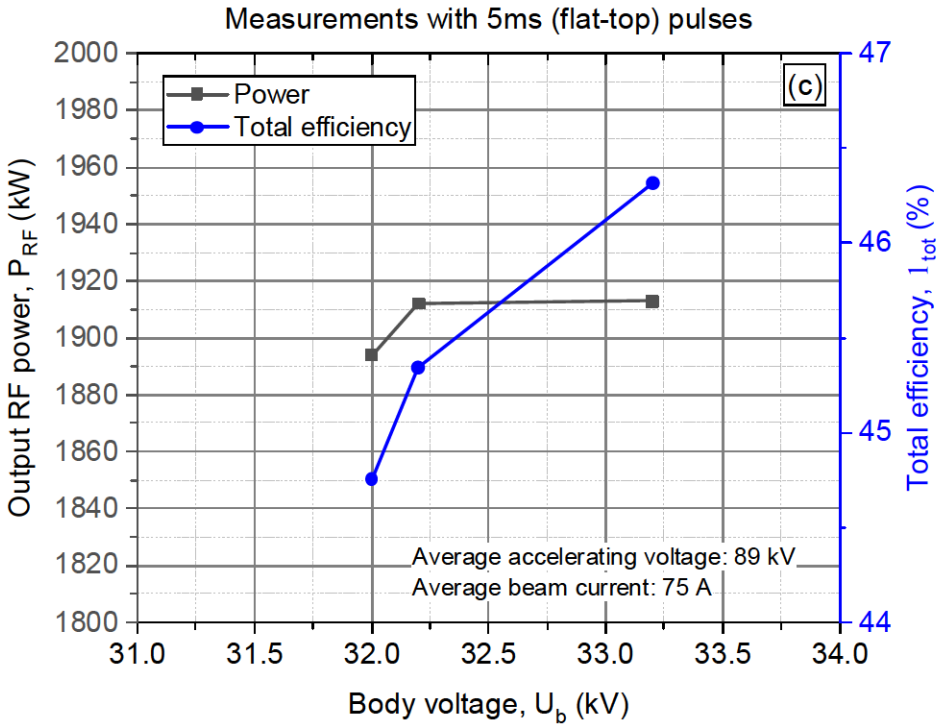

Fig. 1.3.1: Experimental measurements with the coaxial 170 GHz, 2 MW gyrotron. 2 MW – 5 ms (flat-top phase of the pulse).

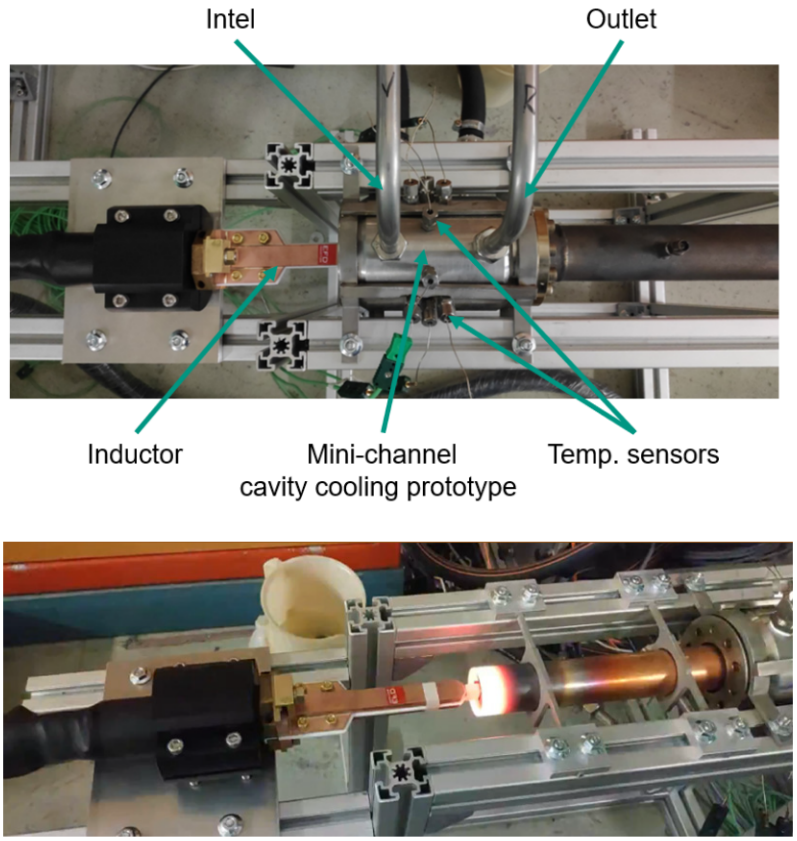

Fig. 1.3.2: Top: test set-up of mini-channel cavity mock-up with induction heating system. Bottom: Initial test, heating up a simple copper pipe.

Since the maximum acceptable heat-load on the cavity wall of fusion gyrotrons is a technological limiting factor for power, efficiency, and pulse-length, studies on advanced cooling systems are ongoing. A mock-up cavity, relevant to the 170 GHz, 2 MW coaxial gyrotron and equipped with mini-channels, has been fabricated. The existing test set-up for the performance analysis of the mock-up has been significantly upgraded by the procurement of an induction heating system, which replaced the gas burner used before. The test set-up, shown in Fig. 1.3.2, is now fully operational and experimental validation of the fabricated cavity mock-up is foreseen for the next period. To check the effectiveness of the induction heating system, a simple copper pipe with 1 mm wall thickness was heated as an initial test. A maximum temperature of more than 700°C at 60 % of the maximum heating power was achieved (Fig. 1.3.2).

To keep the path towards the DEMO gyrotron as fast and cost-effective as possible, the development of a 2 MW, 170/204 GHz coaxial gyrotron is ongoing, using the existing 170 GHz, 2 MW coaxial gyrotron as a starting point. Operation at ~240 GHz is also under investigation. The gyrotron scientific design has been finalized, as far as the coaxial cavity, the non-linear up-taper, and the quasi-optical system are concerned. The expected RF output power from the cavity is 2.67 MW with 39.0 % interaction efficiency at 170 GHz, and 2.12 MW with 35.7 % interaction efficiency at 204 GHz, using the existing triode coaxial Magnetron Injection Gun. Also, 1.65 MW with an interaction efficiency of 33.8 % can be achieved at 237 GHz. The non-linear up-taper after the cavity has been designed using a scattering matrix code to reduce the mode conversion below 0.1 %. In addition, studies on the performance of the design with respect to frequency step-tunability of ± 10 GHz around the centre frequency in steps of 2-3 GHz have been initiated. The frequency step-tunability of the gyrotron is a prerequisite for controlling fusion plasma instabilities by

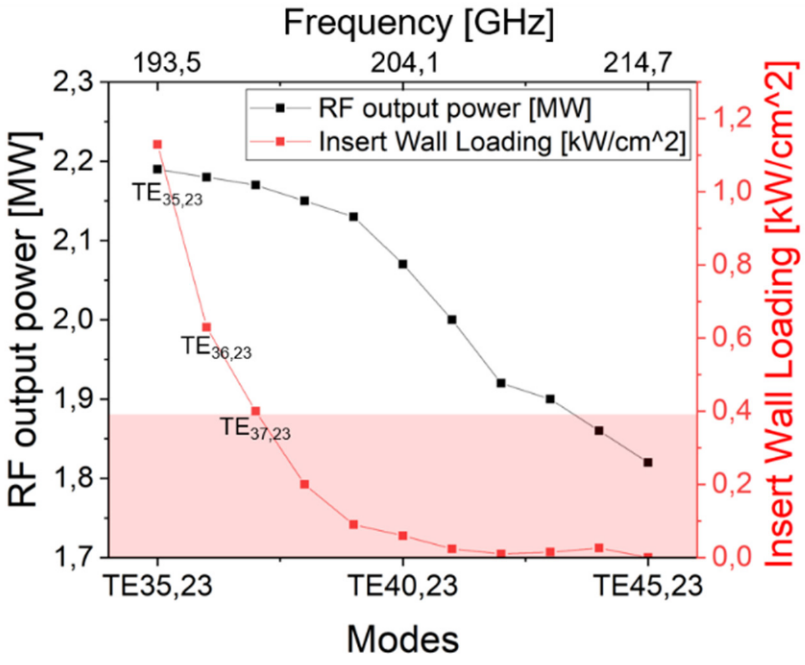

Fig. 1.3.3: Results on possible frequency step-tunability achievable with the dual-frequency design around 204 GHz.

frequency tunable ECRH, as described later in this section. Some results of the initial studies on identification of possible modes and operating points are shown in Fig. 1.3.3. The main challenge is the high insert loading: several modes with a lower azimuthal index show an insert loading above the technological limit of ~0.4 kW/cm^2. Further investigations are foreseen to find different operating regimes and/or different insert designs.

To support the 170/204 GHz coaxial gyrotron development, a mode generator cavity for the $TE_{40,23}$ mode has been designed, fabricated, and tested successfully. The mode was excited at 203.92 GHz with good quality (Fig. 1.3.4). This is the first time the excitation of such a high-order mode is achieved in a mode generator. In parallel, the frequency measurement system in the gyrotron laboratory FULGOR is being upgraded. For gyrotron operation in the 170-240 GHz range, a very broadband (110-260 GHz) frequency measurement setup is under development (see also 1.6.1).

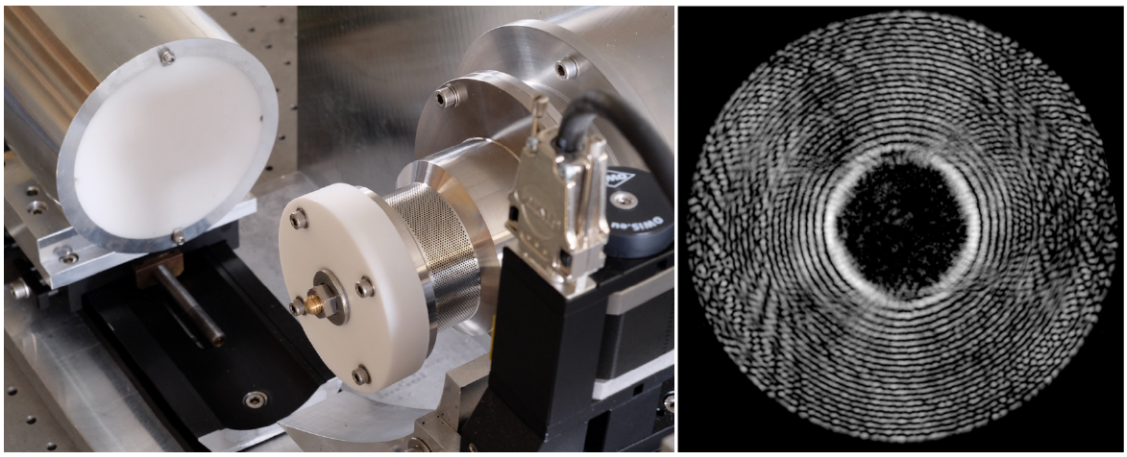

Fig. 1.3.4: Left: Quasi-optical mode generator test-setup for the $TE_{40,23}$ mode. Right: Measured field intensity pattern of the excited $TE_{40,23}$ mode at 203.92 GHz.

Fig. 1.3.5: 3D print of a 1:4 model of a cylindrical two-stage collector design.

The target of ≥ 60 % efficiency for the DEMO gyrotron implies the development of advanced Multi-Stage Depressed Collectors (MDC) to increase the energy recuperation from the spent electron beam. The theoretical studies related to the development of an MDC system for high power gyrotron based on ExB drift concept were continued. A new smaller design was proposed and theoretically investigated. In parallel, a preliminary engineering drawing was developed, whereas a model was manufactured using 3D printing technology (Fig. 1.3.5). The main target is the manufacturing and the experimental test of a full size state-of-the-art multistage depressed collector for high-power gyrotrons.

One important feature of the Electron Cyclotron (EC) heating and current drive is that the MW-level power can be totally absorbed within a small region, where the local gyromotion of the electrons of the plasma is resonant with the wave. Due to this feature, the EC system is crucial for the stabilization of Neoclassical Tearing Modes (NTM), since localised heating and current drive within the magnetic island is required. For the tracking of the islands, the parameters of the EC wave beam need to be dynamically adjusted. Typically, the launching angle of the beam must be adaptable. However, the steering of the launching angle would require either movable mirrors or a remote steering concept, both of which pose significant challenges to the EC launcher design. Another possibility is to tune the frequency of the EC waves, while the launching angle remains fixed, by using frequency step-tunable gyrotrons. Since the EC resonance frequency depends on the magnetic field, which gradually decreases with increasing radius, a tuning of the EC beam frequency can follow the variation of the resonance position. The principle of this steering mechanism is not new, but the feasibility of the frequency steering for EU DEMO has not been extensively studied up to now. This is now investigated in the frame of a dedicated EUROfusion Engineering Grant. The feasibility of frequency steering for the suppression of NTMs is studied in the simulation considering realistic beam parameters (using the beam-tracing code TORBEAM) and the recent NTM model in the transport code ASTRA. The work is being performed in collaboration primarily with CNR, Italy and IPP. One example case for the calculated NTM suppression by controlling the gyrotron frequency can be seen in Fig. 1.3.6.

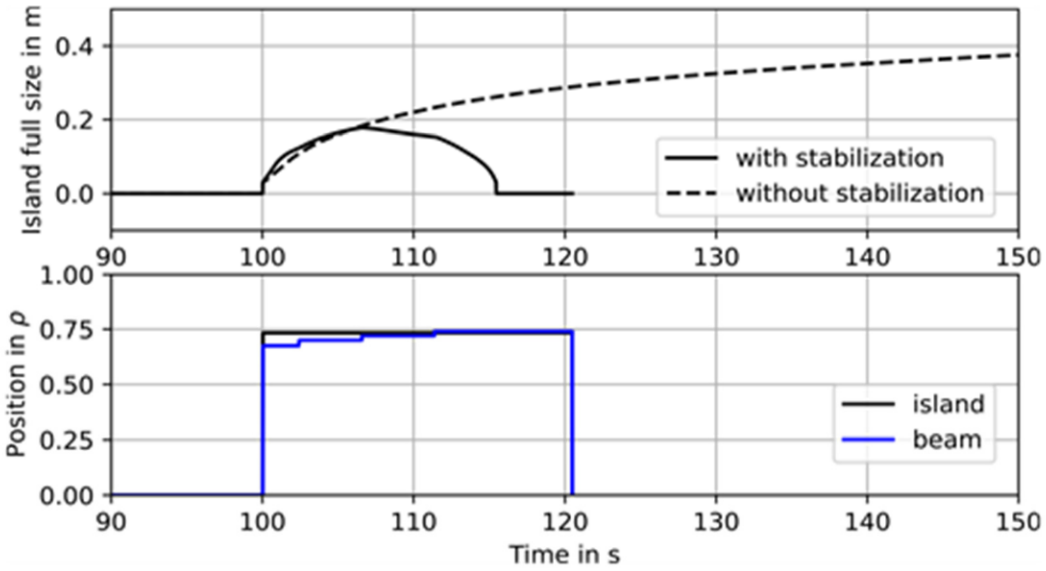

Fig. 1.3.6: Top: Temporal growth of NTM island without EC beam stabilization and with stabilization using a 20 MW frequency step-tunable EC beam. Bottom, blue: Resonance position of the 20 MW EC beam, with respect to the normalized tokamak radius ρ, as the frequency is tuned in time using four steps. (Each step is separated from the previous one by ~3 GHz, which corresponds to the separation of the gyrotron operating modes). Bottom, black: Position of the NTM island. As soon as the island position is matched by the EC resonance position at step 3, the island begins to shrink (compare with figure on top).

1.4 Improvement of Theoretical Methods and Simulation Tools

Contact: Dr. Stefan Illy

1.4.1 Improvements of the KarLESSS code

Our advanced computer code KarLESSS for full-wave simulations of arbitrarily overmoded waveguide components, and of special quasi-optical systems in high-power gyrotrons, was extended by the possibility to simulate Ohmic losses. The simulation method is based on the Skin-Effect and also takes into account the additional losses due to surface roughness. For a validation, we simulated the Ohmic losses on the mirrors of overmoded 90° miter bends and compared our simulations to the measurements performed in earlier publications. The results for a flat stainless steel mirror and a mirror with a λ/8 sinusoidal corrugation are shown in Fig. **1.4.1**. The Ohmic losses for different rotation angles ϕ of the incident linear polarized HE_{11} mode are shown. For a better comparison of measurement and simulation, the shown losses are normalized by the following normalization factor

$$N = \frac{4R_s}{Z_0}$$

with the surface resistance R_s and the free space impedance Z_0. We found a good agreement between measurement and simulation.

A further milestone in the development of KarLESSS is the use of GPUs for all post-processing purposes. Depending on the available hardware, this promises a high speed-up. For example, on a Nvidia GTX 1070 Ti we observe a speed-up of a factor of 2 compared to a powerful dual socket system with two Intel Xeon E5-2640 with a total number of 12 CPU cores operating at 2.5 GHz.

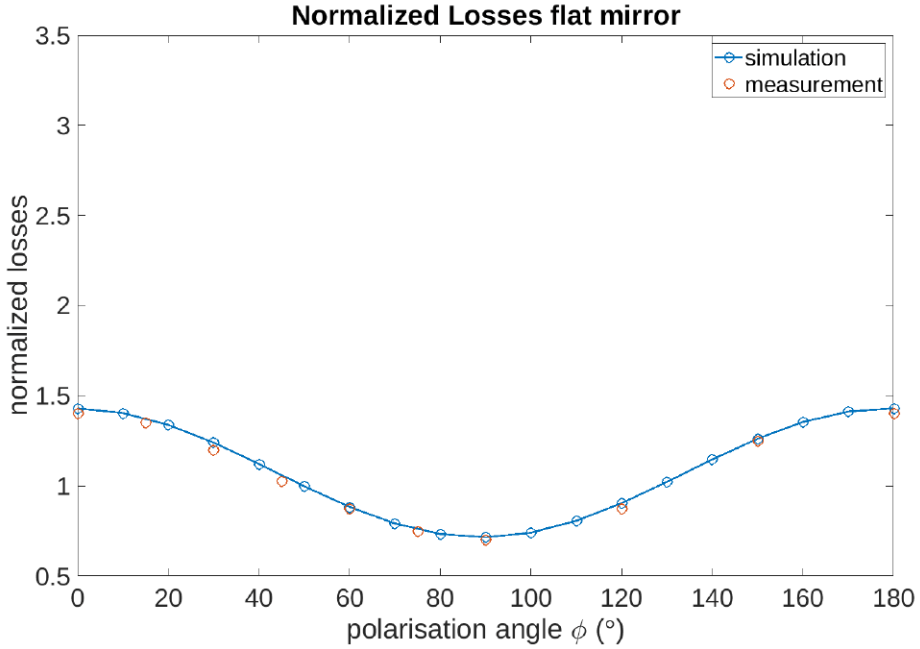

a)

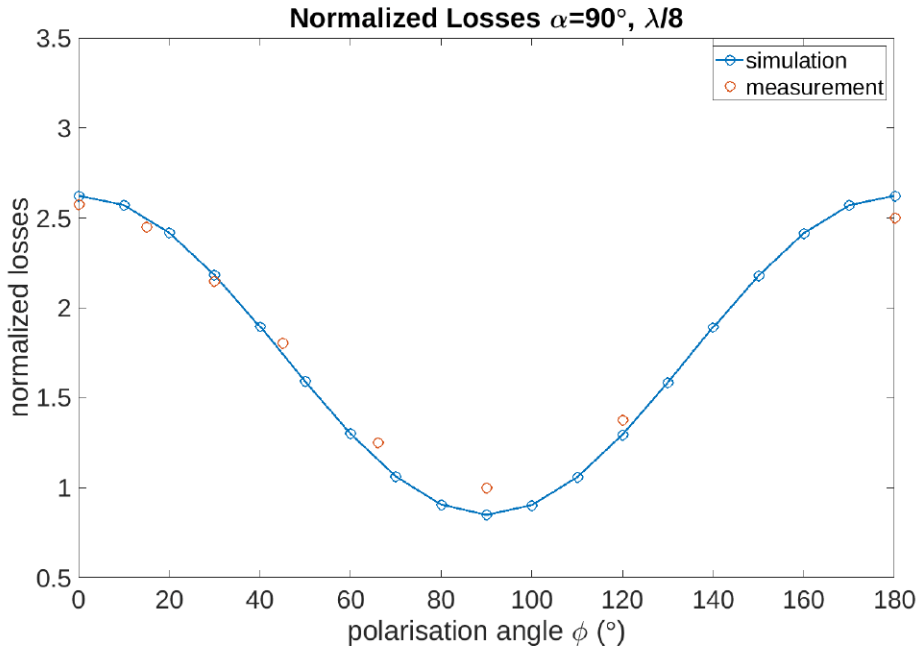

b)

Fig. 1.4.1: Ohmic losses of a plane stainless steel mirror (a) and a mirror with λ/8 sinusoidal corrugations (b) in a 90° miter bend (I.D. = 87 mm, f = 140 GHz) for different angle ϕ of the incident linear polarized HE_{11} mode. Dots: experimental data line: simulation with KarLESSS; data normalized to the case of perpendicular incidence.

1.5 Passive Broadband Microwave Components

Contact: M.Sc. Daniel Haas

1.5.1 Polarizer Miter Bends

Polarizer miter bends are used to alter the polarization in overmoded waveguides. For future broadband applications, like Dynamic Nuclear Polarization (DNP) or Nuclear Magnetic Resonance (NMR) spectroscopy, these are important system components. A polarizer miter bend uses a grooved mirror as phase grid for modification of the polarization. At IHM, KIT, a suitable design of such a phase grid for broadband applications within the frequency range from 90 GHz to 100 GHz were investigated. An optimized parameter combination for a circular polarizer was found by a parametric study. For the reduction of the numerical efforts a plane wave approximation and unit cell simulations were used (cf. Fig. 1.5.1). With the optimized parameter combination, a cross polarization below -26 dB could be achieved within the considered frequency range. This leads to an excellent polarization quality. Ass shown in Fig. 1.5.2, the corresponding polarization losses are always less than 0.25 %.

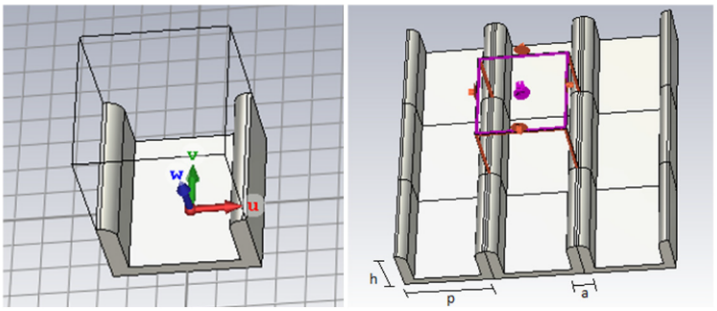

(a) (b)

Fig. 1.5.1: Simulation model: (a) unit cell; (b) details of the extended phase grid (a =0.25 mm, p = 1 mm, h = 0.48 mm).

Future research activities will address the mode purity and the exact mode content at the output of a polarizer miter bend. Spurious modes may degrade the cross polarization or the phase stability. For high performance applications, like DNP/NMR-spectroscopy, these effects have to take into account.

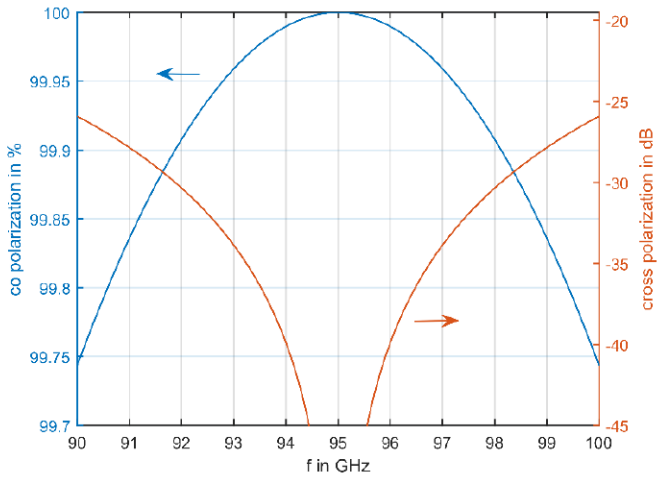

Fig. 1.5.2: Co and cross polarization of an optimized phase grid (simulations).

1.6 FULGOR (Fusion Long-Pulse Gyrotron Laboratory)

Contact: Dr. Gerd Gantenbein

The existing gyrotron test facility at KIT, which had been designed and built about 35 years ago, plays a worldwide leading role in the development of high-power gyrotrons for nuclear fusion applications. This facility offered the unique opportunity to develop and test the first CW high power series gyrotrons for the stellarator W7-X in collaboration with IPP and Thales Electron Devices as the industrial partner.

The target parameters of the new gyrotron test facility are well beyond the capabilities of the existing one. The new teststand will strongly support KIT's leading role in the development of advanced gyrotrons. It will help to answer the questions regarding the technical limits and new physical designs for future high-power microwave tubes. The key parameters of FULGOR will be:

- Full CW operation with up to 10 MW electrical power (, corresponding to >= 4 MW RF power (assuming an efficiency of the gyrotron >= 40 %)
- Support of advanced energy recovery concepts, e.g. multi-stage depressed collector (MSDC)

The high voltage power supply (HVPS) will support an operating voltage of up to 130 kV with up to 120 A beam current in short pulse operation and 90 kV / 120 A in continues wave regime. A superconducting magnet which allows operation of gyrotrons at frequencies well above 200 GHz will be a major component of FULGOR. Other significant components of the teststand are: cooling system, control electronics and interlock system, RF diagnostics including high-power RF absorber loads.

The capabilities of FULGOR will enable the development and CW tests of gyrotrons for future fusion machines like ITER and DEMO. Fig. 1.6.1 is a simplified CAD view of the complete FULGOR system and the status of installation.

Substantial progress has been achieved in the field of diagnostics, fast data acquisitation and procurement of the superconducting magnet.
The calorimetric diagnostics of the microwave box has been installed completely, including a 2 MW RF absorber load. The procurement of the fast data acquisition system has been finalized. The procurement of components and the production of the body power supply is ongoing.

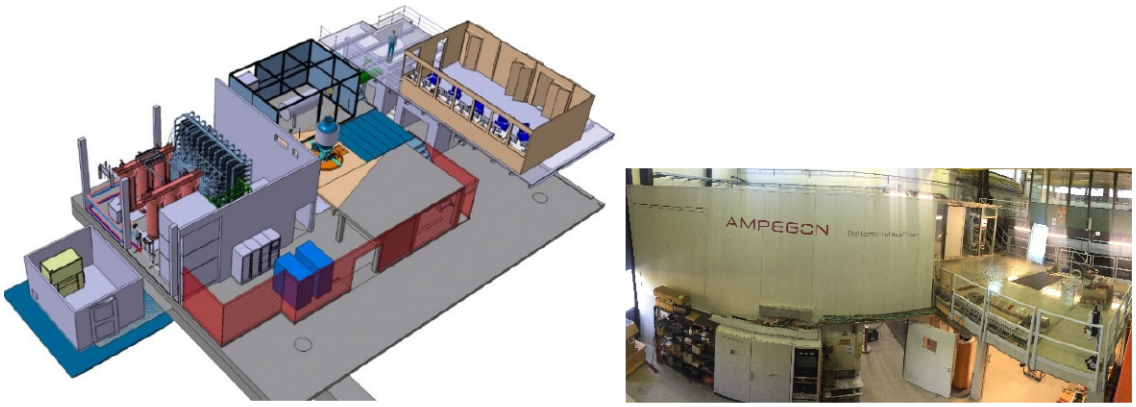

Fig. 1.6.1: RF Diagnostics for FULGOR CAD view of FULGOR teststand and status of installation.

Superconducting magnet: This is a very challenging component since the requirements are beyond what is industrial standard. In 2019 all major components have been manufactured, at the premise of the manufacturer, TESLA Ltd., GB, the assembling of the cold mass has been started and is in an advanced status.

1.6.1 RF Diagnostics for FULGOR

The frequency measurement system (FMS) in the existing gyrotron laboratory is limited to 175 GHz. However, gyrotrons up to 240 GHz or even higher can operate in the FULGOR test stand. This requires a new frequency measurement system which consists of two sub-systems. First, the FMS system, which includes a filterbank and a modulation domain analyser after the down conversion of the gyrotron frequency to an intermediate frequency (IF) with a RF mixer. The filterbank has an IF-range of up to 20 GHz with a resolution of 2 GHz and an expected dynamic range of 29 dB for a broadband overview of the operation behaviour of the gyrotron. In parallel, a modulation domain analyser with a bandwidth of 3 GHz and a frequency resolution of 100 kHz and an expected dynamic range of 25 dB is considered for a precise evaluation of the operating mode or spurious modes. The benefit of the setup is the fast evaluation of the frequency in real time. The status on the upgrade is shown in Fig. 1.6.2. The IF-components, power supply and signal generators were installed in a 19 inch rack. The missing RF mixers will be delivered in 2020. The final system will be capable to operate in a frequency range of 110-260 GHz.

The second system, a PSA (Pulse Spectrum Analysis) is a high performance analysis of the frequency with a dynamic range of 60 dB and an IF bandwidth of up to 12 GHz, where parasitic oscillations, modulation and competing modes can be detected. The RF mixers working on the 14^{th} and 16^{th} harmonic will be delivered in 2020.

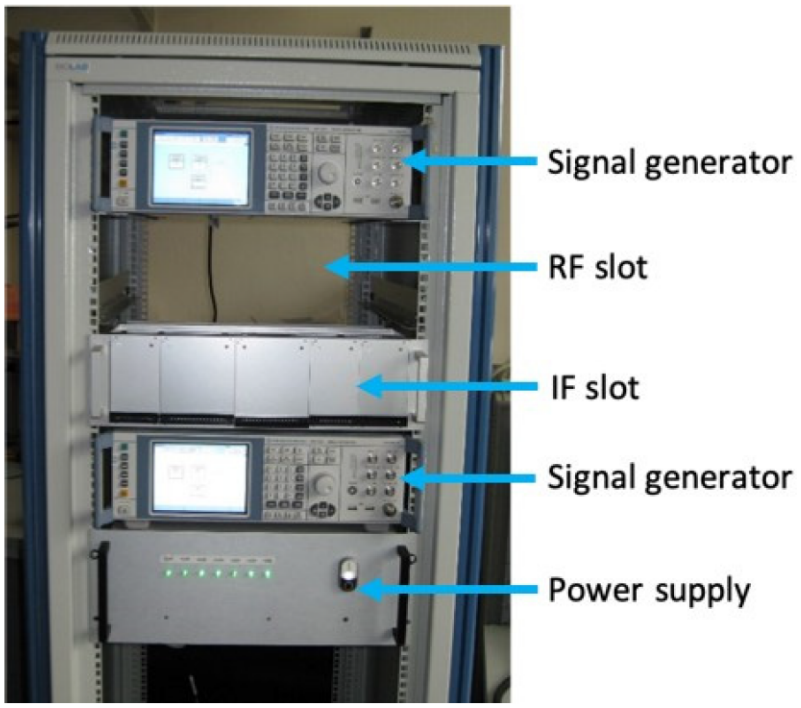

Fig. 1.6.2: Photo on the Status of the frequency measurement setup for FULGOR. The signal generator, power supply and IF components are tested and installed. The missing RF mixers will be delivered in 2020 and will be installed in the RF slot.

1.7 Experimental study of the gyrotron gun's emission properties – preliminary results

Contact: Dr. Zisis Ioannidis

The quality of the electron beam generated by a Magnetron Injection Gun (MIG) is very important for the performance of high-power, high-frequency gyrotrons. In practice, several parameters such as mechanical misalignments during assembly, manufacturing tolerances, temperature inhomogeneity and emitter roughness, significantly affect the expected performance of the MIG. For this reason, it is important to measure the electron properties of the MIG. To support the characterization of the emission properties of the electron guns a diagnostic device has been designed, based on the principle of the retarding field method, and build at IHM (Fig. 1.7.1). The diagnostic device allows for different measurements: (1) characterization of the azimuthal homogeneity of the emission and (2) estimation the of the pitch factor distribution of the electrons at specific azimuthal position.

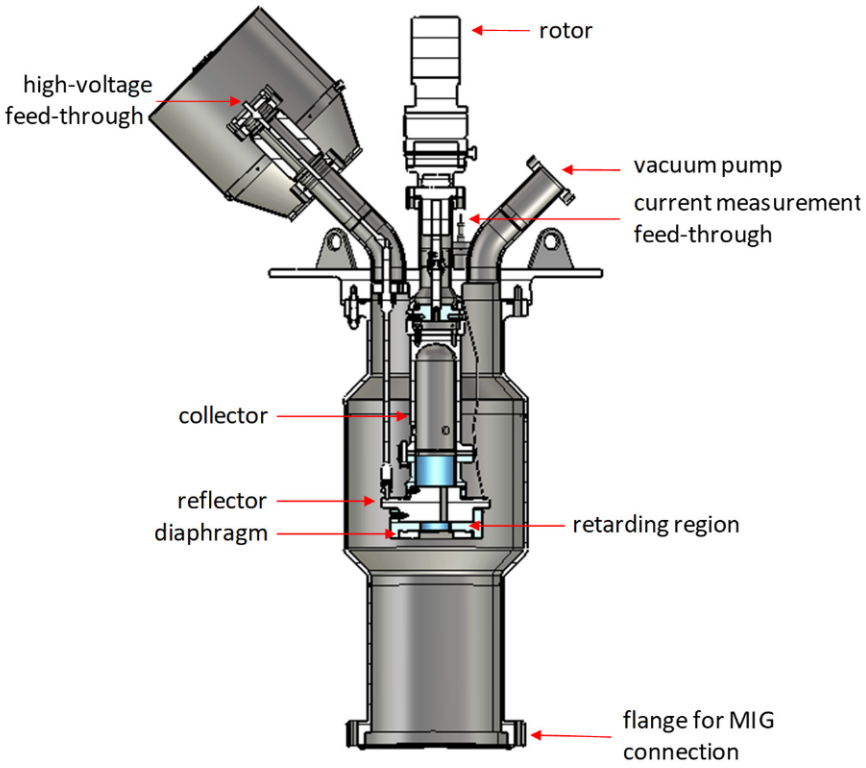

Fig. 1.7.1: First prototype of the electron beam-tester prototype.

As a first test we used a diode MIG which has been used for several years with a prototype gyrotron. It is assumed that the MIG is approaching the end of its lifetime. The preliminary experiments with the MIG focused on the study of the emission homogeneity, at scaled down beam parameters. Fig. 1.7.2 presents the measured current at the collector with respect to the azimuthal position of the diaphragm's slot (zero angle is arbitrarily selected). For each curve the current has been first normalized to the total beam current (sum of the diaphragm and collector current) and then to the maximum value of all measurements. Each curve has progressively lower average pitch-factor value than the previous one, according to simulation. This choice is made to minimize the chance of having reflected electrons. It is interesting to note that the collected current depends strongly on the azimuthal position of the diaphragm's slot. It is easy to identify

five azimuthal positions with relatively high emission, while in between of them there are areas with minimal or practically zero emission. This phenomenon could be attributed either to a strong temperature inhomogeneity of the surface of the emitter or to excessive oxidation/poisoning of areas of the emitter surface. In any of these cases, the intense variation of the current with respect to the azimuthal position can create instabilities to the beam and significantly affect the properties of the electrons. Further investigation on other MIGs and on the device itself is in progress.

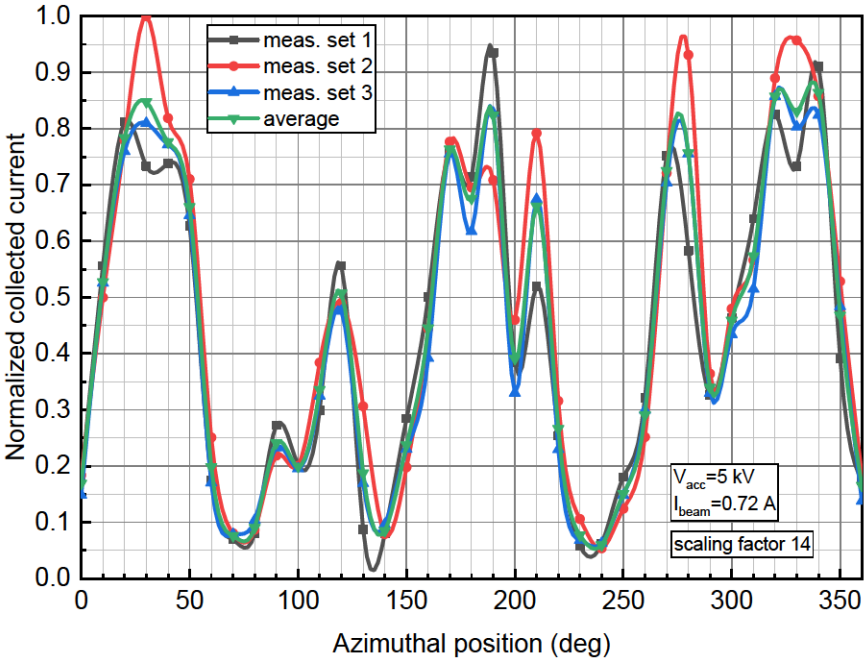

Fig. 1.7.2: Measured collected current with respect to the azimuthal position of the diaphragm opening.

1.8 Generation of ultra-short pulses with new gyro-devices

Contact: M.Sc. Alexander Marek

A new type of pulsed sources in the millimeter and sub-millimeter frequency range, utilizing the method of passive mode locking, is proposed in 2015 from the Institute of Applied Physics (IAP-RAS) in Nizhny Novgorod and studied in a joint RSF-DFG project from the IHM and the IAP-RAS. The need for new powerful pulsed sources of millimeter and sub-millimeter (sub-THz) radiation is motivated by a large number of fundamental problems and practical applications, as diagnostics of plasma, photochemistry, biophysics, new locating systems, and the spectroscopy of various media.

The principle of passive mode locking, well known from laser physics, allows the generation of a periodic series of powerful, coherent, ultra-short pulses. A realization for millimeter and sub-millimeter waves consists of an amplifier and a saturable absorber coupled in a feedback loop. For the generation of powerful, sub-ns pulses at sub-THz frequencies, the active devices, namely the amplifier and absorber, must fulfill challenging properties, such as the demand for a high bandwidth at high power. A promising technology for the amplifier as well as the absorber are gyrotron traveling-wave tubes (gyro-TWTs) with helical interaction region. This type of vacuum tubes provide a series of advantages compared to classical gyro-TWTs based on cylindrical interaction circuits with dielectric losses. The helical gyro-TWTs provide a higher bandwidth and can operate at lower magnetic fields because the electron-wave interaction takes place at the 2nd cyclotron harmonic. This is of particular interest for the development of devices in the sub-THz range, where the required magnetic field strength for operation at the fundamental cyclotron harmonic can easily exceed 10 T.

As the amplifier and saturable absorber can only be realized in two separate gyro-TWTs, a new feedback system for a passive mode locked pulsed oscillator at 263 GHz is developed (see Fig. 1.8.1). It couples effectively the two gyro-devices and enables the decoupling of the output signal. The design shown fulfills all the necessary requirements: high bandwidth (10 GHz), variable decoupling of the output signal, low losses and a separation of the signal paths “amplifier-to-absorber” and “absorber-to-amplifier” for an improved stability of passive mode locked oscillator.

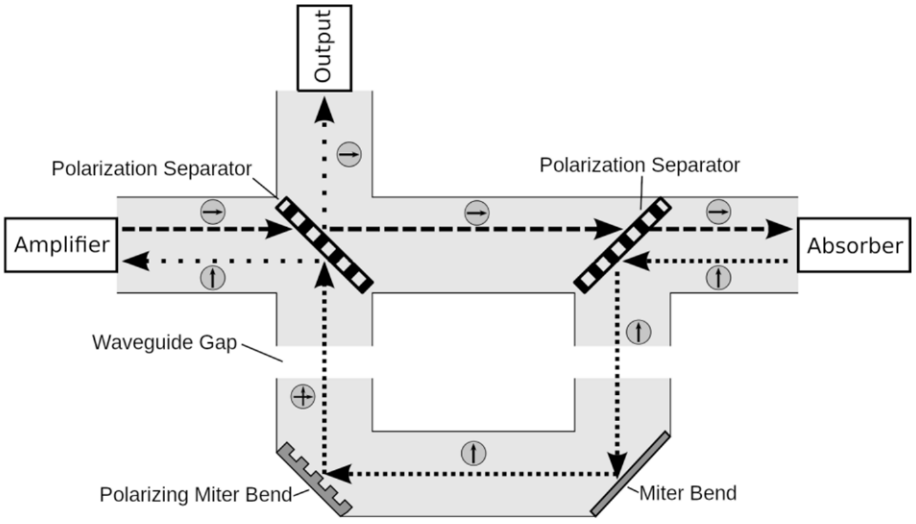

Fig. 1.8.1: Amplifier and absorber devices working with single input-output window coupled by corrugated, overmoded waveguides. The arrows symbolize the polarization of the HE_{11} mode.

In the past years of the project, we successfully investigated in the usage of the advanced simulation program “PICLas” (originally developed by the Institute of Aerodynamics and Gas Dynamics at the University of Stuttgart) for the electron-wave interaction in helical gyro-devices. Going a first step closer to a faster synthesis of new interaction circuits, we currently work on the development of a simplified model for the interaction simulation.

Involved Staff:

KIT/IHM: D. Albert, Dr. K. Avramidis, B. Ell, D. Haas, **Dr. G. Gantenbein, Dr. S. Illy**, Dr. Z. Ioannidis, Prof. J. Jelonnek, Dr. J. Jin, Dr. P. Kalaria, Th. Kobarg, R. Lang, W. Leonhardt, A. Marek, G. Marschall, D. Mellein, A. Meier (KIT, IAM-AWP), Dr. I. Pagonakis, A. Papenfuß, T. Ruess, **Dr. T. Rzesnicki**, Prof. Dr. Theo A. Scherer (KIT, IAM-AWP), M. Schmid, Dr. S. Stanculovic, Dr. D. Strauss (KIT, IAW-AWP), Prof. M. Thumm, J. Weggen, Dr. Ch. Wu, **IGVP (University of Stuttgart): Dr. C. Lechte**, R. Munk, Dr. B. Plaum, B. Roth, A. Zeitler, **IPP (Greifswald/Garching):** Dr. H. Braune, F. Hollmann, **Dr. H. Laqua**, Dr. S. Marsen, F. Noke, F. Purps, T. Schulz, Dr. T. Stange, P. Uhren

Journal Publications

W7-X Team; Abramovic, I.; Pavone, A.; Moseev, D.; Lopes Cardozo, N. J.; Salewski, M.; Laqua, H. P.; Stejner, M.; Stange, T.; Marsen, S.; Nielsen, S. K.; Jensen, T.; Kasparek, W.; Baumann, K.; Dammertz, G.; Fietz, W. H.; Gantenbein, G.; Huber, M.; Hunger, H.; Illy, S.; Jelonnek, J.; Kobarg, T.; Lang, R.; Leonhardt, W.; Losert, M.; Meier, A.; Mellein, D.; Papenfuß, D.; Samartsev, A.; Scherer, T.; Schlaich, A.; Spiess, W.; Thumm, M.; Wadle, S.; Weggen, J. (2019). Forward modeling of collective Thomson scattering for Wendelstein 7-X plasmas: Electrostatic approximation. Review of scientific instruments, 90 (2), 023501.

Aiello, G.; Scherer, T.; Avramidis, K.; Casal, N.; Franke, T.; Gagliardi, M.; Gantenbein, G.; Henderson, M.; Jelonnek, J.; Meier, A.; Saibene, G.; Schreck, S.; Strauss, D.; Thumm, M.; Tran, M. Q.; Wild, C.; Woerner, E. (2019). Diamond Window Technology for Electron Cyclotron Heating and Current Drive: State of the Art. Fusion science and technology, 75 (7), 719–729.

Avramidis, K. A.; Aiello, G.; Alberti, S.; Brücker, P. T.; Bruschi, A.; Chelis, I.; Franke, T.; Gantenbein, G.; Garavaglia, S.; Genoud, J.; George, M.; Granucci, G.; Grossetti, G.; Hogge, J.-P.; Illy, S.; Ioannidis, Z. C.; Jelonnek, J.; Jin, J.; Kalaria, P. C.; Latsas, G. P.; Marek, A.; Pagonakis, I. G.; Peponis, D. V.; Ruess, S.; Ruess, T.; Rzesnicki, T.; Scherer, T.; Schmid, M.; Strauss, D.; Thumm, M.; Tigelis, I.; Wu, C.; Zein, A.; Zisis, A.; Tran, M. Q. (2019). Overview of recent gyrotron R&D towards DEMO within EUROfusion Work Package Heating and Current Drive. Nuclear fusion, 59 (6), Article no: 066014.

Avramidis, K. A.; Ruess, T.; Mentgen, F.; Jin, J.; Wagner, D.; Gantenbein, G.; Illy, S.; Ioannidis, Z. C.; Laqua, H. P.; Pagonakis, I. G.; Rzesnicki, T.; Thumm, M.; Wolf, R. C.; Jelonnek, J. (2019). Studies towards an upgraded 1.5 MW gyrotron for W7-X. (E. Poli, H. Laqua & J. Oosterbeek, Hrsg.)The European physical journal / Web of Conferences, 203, Art. Nr.: 04003.

W7-X Team; Baldzuhn, J.; Damm, H.; Beidler, C. D.; McCarthy, K.; Panadero, N.; Biedermann, C.; Bozhenkov, S. A.; Brunner, K. J.; Fuchert, G.; Kazakov, Y.; Beurskens, M.; Dibon, M.; Geiger, J.; Grulke, O.; Höfel, U.; Klinger, T.; Köchl, F.; Knauer, J.; Kocsis, G.; Kornejew, P.; Lang, P. T.; Langenberg, A.; Laqua, H.; Pablant, N. A.; Pasch, E.; Pedersen, T. S.; Ploeckl, B.; Rahbarnia, K.; Schlisio, G.; Scott, E. R.; Stange, T.; von Stechow, A.; Szepesi, T.; Turkin, Y.; Wagner, F.; Winters, V.; Wurden, G.; Zhang, D.; Gantenbein, G.; Huber, M.; Hunger, H.; Illy, S.; Jelonnek, J.; Kobarg, T.; Lang, R.; Leonhardt, W.; Losert, M.; Meier, A.; Mellein, D.; Papenfuß, D.; Samartsev, A.; Scherer, T.; Schlaich, A.; Spiess, W.; Thumm, M.; Wadle, S.; Weggen, J. (2019). Pellet fueling experiments in Wendelstein 7-X. Plasma physics and controlled fusion, 61 (9), Art.Nr.: 095012.

Bertinetti, A.; Albajar, F.; Avramidis, K. A.; Cau, F.; Cismondi, F.; Gantenbein, G.; Jelonnek, J.; Kalaria, P. C.; Ruess, S.; Rzesnicki, T.; Savoldi, L.; Zanino, R. (2019). Analysis of an actively-cooled coaxial cavity in a 170 GHz 2 MW gyrotron using the multi-physics computational tool MUCCA. Fusion engineering and design, 146A, 74–77.

Bin, W.; Bruschi, A.; Fanale, F.; Francesca, M.; Lucca, F.; Albajar, F.; Alberti, S.; Carannante, G.; Cavinato, M.; Chelis, I.; Dell'Era, F.; Fasel, D.; Gantenbein, G.; Goodman, T.; Granucci, G.; Hogge, J.-P.; Ikeda, R.; Ioannidis, Z.; Legrand, F.; Mellera, V.; Minelli, D.; Nardone, A.; Pagonakis, I.; Rispoli, N.; Rzesnicki, T.; Sanchez, F.; Spinicchia, N.; Takahashi, K.; Tigelis, I.; Viganò, F. (2019). Tests and developments of a long-pulse high-power 170 GHz absorbing matched load. Fusion engineering and design, 146A, 36–39.

Dinklage, A.; McCarthy, K. J.; Suzuki, C.; Tamura, N.; Wegner, T.; Yamada, H.; Baldzuhn, J.; Brunner, K. J.; Buttenschön, B.; Damm, H.; Drewelow, P.; Fuchert, G.; Hirsch, M.; Hoefel, U.; Kasahara, H.; Knauer, J.; Maier, D.; Miyazawa, J.; Motojima, G.; Oishi, T.; Rahbarnia, K.; Sunn Pedersen, T.; Sakamoto, R.; Wolf, R. C.; Zhang, D.; Gantenbein, G.; Huber, M.; Hunger, H.; Illy, S.; Jelonnek, J.; Kobarg, T.; Lang, R.; Leonhardt, W.; Losert, M.; Meier, A.; Mellein, D.; Papenfuß, D.; Samartsev, A.; Scherer, T.; Schlaich, A.; Spiess, W.; Thumm, M.; Wadle, S.; Weggen, J. (2019). Plasma termination by excess pellet fueling and impurity injection in TJ-II, the Large Helical Device and Wendelstein 7-X. Nuclear fusion, 59 (7), 076010.

Ell, B.; Pagonakis, I. G.; Wu, C.; Thumm, M.; Jelonnek, J. (2019). Coaxial multistage depressed collector design for high power gyrotrons based on E×B concept. Physics of plasmas, 26 (11), 113107.

W7-X Team; Geiger, B.; Wegner, T.; Beidler, C. D.; Burhenn, R.; Buttenschön, B.; Dux, R.; Langenberg, A.; Pablant, N. A.; Pütterich, T.; Turkin, Y.; Windisch, T.; Winters, V.; Beurskens, M.; Biedermann, C.; Brunner, K. J.; Cseh, G.; Damm, H.; Effenberg, F.; Fuchert, G.; Grulke, O.; Harris, J. H.; Killer, C.; Knauer, J.; Kocsis, G.; Krämer-Flecken, A.; Kremeyer, T.; Krychowiak, M.; Marchuk, O.; Nicolai, D.; Rahbarnia, K.; Satheeswaran, G.; Schilling, J.; Schmitz, O.; Schröder, T.; Szepesi, T.; Thomsen, H.; Trimino Mora, H.; Traverso, P.; Zhang, D.; Baumann, K.; Dammertz, G.; Gantenbein, G.; Huber, M.; Hunger, H.; Illy, S.; Jelonnek, J.; Kobarg, T.; Lang, R.; Leonhardt, W.; Losert, M.; Mellein, D.; Papenfuß, D.; Smartsev, A.; Scherer, T.; Schlaich, A.; Spieß, W.; Thumm, M.; Wadle, S.; Weggen, J. (2019). Observation of anomalous impurity transport during low-density experiments in W7-X with laser blow-off injections of iron. Nuclear fusion, 59 (4), 046009.

Genoud, J.; Alberti, S.; Tran, T. M.; Le Bars, G.; Kaminski, P.; Hogge, J.-P.; Avramidis, K. A.; Tran, M. Q. (2019). Parasitic Oscillations in Smooth-Wall Circular Symmetric Gyrotron Beam Ducts. Journal of infrared, millimeter, and terahertz waves, 40 (2), 131–149.

Girka, I. O.; Pavlenko, I. V.; Thumm, M. (2019). Electromagnetic energy rotation by azimuthal surface waves along plasma-metal interface around a cylindrical metallic rod placed into infinite magnetized plasma. Physics of plasmas, 26 (5), 052103.

Girka, I. O.; Pavlenko, I. V.; Thumm, M. (2019). Electromagnetic energy rotation along plasma-metal interface in cylindrical waveguides initiated by azimuthal surface waves. Physics of plasmas, 26 (2), 022113.

Girka, I. O.; Girka, O. I.; Thumm, M. (2019). Initial stage of interaction between gyrating relativistic electron beam and long-wavelength electromagnetic surface waves in cylindrical metallic waveguides partially filled with plasma. Physics of plasmas, 26, 042118.

W7-X Team; Hoefel, U.; Hirsch, M.; Kwak, S.; Pavone, A.; Svensson, J.; Stange, T.; Hartfuß, H.-J.; Schilling, J.; Weir, G.; Oosterbeek, J. W.; Bozhenkov, S.; Braune, H.; Brunner, K.-J.; Chaudhary, N.; Damm, H.; Fuchert, G.; Knauer, J.; Laqua, H.; Marsen, S.; Moseev, D.; Pasch, E.; Scott, E. R.; Wilde, F.; Wolf, R.; Baumann, K.; Dammertz, G.; Fietz, W. H.; Gantenbein, G.; Huber, M.; Hunger, H.; Illy, S.; Jelonnek, J.; Kobarg, T.; Lang, R.; Leonhardt, W.; Losert, M.; Meier, A.; Mellein, D.; Papenfuß, D.; Samartsev, A.; Scherer, T.; Schlaich, A.; Spiess, W.; Thumm, M.; Wadle, S.; Weggen, J. (2019). Bayesian modeling of microwave radiometer calibration on the example of the Wendelstein 7-X electron cyclotron emission diagnostic. Review of scientific instruments, 90 (4), 043502.

Illy, S.; Avramidis, K. A.; Gantenbein, G.; Ioannidis, Z. C.; Jin, J.; Kalaria, P. C.; Pagonakis, I. G.; Ruess, S.; Ruess, T.; Rzesnicki, T.; Thumm, M.; Jelonnek, J. (2019). Recent Status and Future Prospects of Coaxial-Cavity Gyrotron Development at KIT. (E. Poli, H. Laqua & J. Oosterbeek, Hrsg.)The European physical journal / Web of Conferences, 203, Art.Nr.: 04005.

Ioannidis, Z. C.; Albajar, F.; Alberti, S.; Avramidis, K. A.; Bin, W.; Bonicelli, T.; Bruschi, A.; Chelis, J.; Fanale, F.; Gantenbein, G.; Genoud, J.; Hogge, J.-P.; Hermann, V.; Illy, S.; Jelonnek, J.; Jin, J.; Kasparek, W.; Latsas, G. P.; Legrand, F.; Lechte, C.; Pagonakis, I. G.; Rzesnicki, T.; Sánchez, F.; Schlatter, C.; Schmid, M.; Tigelis, I. G.; Thumm, M.; Tran, M. Q.; Zisis, A.; Zein, A. (2019). Recent experiments with the European 1MW, 170GHz industrial CW and short-pulse gyrotrons for ITER. Fusion engineering and design, 146 (Part A), 349–352. doi:10.1016/j.fusengdes.2018.12.065

Ioannidis, Z. C.; Avramidis, K. A.; Gantenbein, G.; Illy, S.; Kobarg, T.; Pagonakis, I. G.; Rzesnicki, T.; Jelonnek, J. (2019). Development and Experimental Verification of an XY-Table for the Optimization of the Alignment of High-Power Gyrotrons. IEEE transactions on electron devices, 66 (4), 1954–1959.

Ioannidis, Z. C.; Rzesnicki, T.; Albajar, F.; Alberti, S.; Avramidis, K. A.; Bin, W.; Bonicelli, T.; Bruschi, A.; Chelis, I.; Fanale, F.; Gantenbein, G.; Hermann, V.; Hogge, J.-P.; Illy, S.; Jin, J.; Jelonnek, J.; Kasparek, W.; Latsas, G.; Lechte, C.; Legrand, F.; Pagonakis, I.; Sanchez, F.; Schmid, M.; Schlatter, C.; Thumm, M.; Tigelis, I.; Tran, M. Q.; Zisis, A.; Zein, A. (2019). Report of recent experiments with the European 1 MW, 170 GHz CW and SP prototype gyrotrons for ITER. (E. Poli, H. Laqua & J. Oosterbeek, Hrsg.)The European physical journal / Web of Conferences, 203, 04006.

Jelonnek, J.; Aiello, G.; Alberti, S.; Avramidis, K. A.; Bruschi, A.; Chelis, I.; Franke, T.; Gantenbein, G.; Garavaglia, S.; Granucci, G.; Grossetti, G.; Illy, S.; Ioannidis, Z. C.; Jin, J.; Kalaria, P.; Latsas, G.; Pagonakis, I.; Peponis, D.; Rzesnicki, T.; Ruess, S.; Ruess, T.; Scherer, T.; Schmid, M.; Strauss, D.; Wu, C.; Thumm, M.; Tigelis, I.; Tran, M. Q.; Wilde, F.; Zein, A. (2019). Towards Advanced Fusion Gyrotrons: 2018 Update on Activities within EUROfusion. (E. Poli, H. Laqua & J. Oosterbeek, Hrsg.)The European physical journal / Web of Conferences, 203, 04007.

Jin, J.; Gantenbein, G.; Rzesnicki, T.; Thumm, M.; Jelonnek, J. (2019). Improved Simulation of Quasi-Optical Launchers for High Power Gyrotrons with Smoothing Algorithm. (E. Poli, H. Laqua & J. Oosterbeek, Hrsg.)The European physical journal / Web of Conferences, 203, 04008.

W7-X Team; Killer, C.; Gao, Y.; Perseo, V.; Rudischhauser, L.; Hammond, K.; Buttenschön, B.; Barbui, T.; Blackwell, B. D.; Brunner, K.-J.; Drews, P.; Endler, M.; Geiger, J.; Grulke, O.; Jakubowski, M.; Klose, S.; Knauer, J.; Knieps, A.; König, R.; Li, Y.; Neuner, U.; Niemann, H.; Otte, M.; Schilling, J.; Sitjes, A. P.; Rahbarnia, K.; Stange, T.; Gantenbein, G.; Huber, M.; Hunger, H.; Illy, S.; Jelonnek, J.; Kobarg, T.; Lang, R.; Leonhardt, W.; Losert, M.; Meier, A.; Mellein, D.; Papenfuß, D.; Samartsev, A.; Scherer, T.; Schlaich, A.; Spiess, W.; Thumm, M.; Wadle, S.; Weggen, J. (2019). Effect of toroidal plasma currents on the Wendelstein 7-X Scrape-Off Layer. Plasma physics and controlled fusion, 61 (12), 125014.

Klinger, T.; Andreeva, T.; Bozhenkov, S. A.; Brandt, C.; Burhenn, R.; Buttenschön, B.; Fuchert, G.; Geiger, B.; Grulke, O.; Laqua, H. P.; Pablant, N. A.; Rahbarnia, K.; Stange, T.; von Stechow, A.; Tamura, N.; Thomsen, H.; Wegner, T.; Bussiahn, R.; Gantenbein, G.; Huber, M.; Hunger, H.; Illy, S.; Jelonnek, J.; Kobarg, T.; Lang, R.; Leonhardt, W.; Losert, M.; Meier, A.; Mellein, D.; Papenfuß, D.; Samartsev, A.; Scherer, T.; Schlaich, A.; Spiess, W.; Thumm, M.; Wadle, S.; Weggen, J. (2019). Overview of first Wendelstein 7-X high-performance operation. Nuclear fusion, 59 (11), Article no: 112004.

Krämer-Flecken, A.; Han, X.; Windisch, T.; Cosfeld, J.; Drews, P.; Fuchert, G.; Geiger, J.; Grulke, O.; Killer, C.; Knieps, A.; Liang, Y.; Liu, S.; Rack, M.; Gantenbein, G.; Jelonnek, J.; Thumm, M.; Dammertz, G.; Hunger, H.; Illy, S.; Kern, S.; Prinz, O.; Schmid, M.; Samartsev, A. (2019). Investigation of turbulence rotation and radial

electric field in the island divertor and plasma edge at W7-X. Plasma physics and controlled fusion, 61 (5), 054003.

Langenberg, A.; Warmer, F.; Fuchert, G.; Marchuk, O.; Dinklage, A.; Wegner, T.; Alonso, J. A.; Bozhenkov, S.; Brunner, K. J.; Burhenn, R.; Buttenschön, B.; Drews, P.; Geiger, B.; Grulke, O.; Hirsch, M.; Höfel, U.; Hollfeld, K. P.; Killer, C.; Knauer, J.; Krings, T.; Kunkel, F.; Neuner, U.; Offermanns, G.; Pablant, N. A.; Pasch, E.; Rahbarnia, K.; Satheeswaran, G.; Schilling, J.; Schweer, B.; Thomsen, H.; Traverso, P.; Wolf, R. C.; Baumann, K.; Dammertz, G.; Fietz, W. H.; Gantenbein, G.; Huber, M.; Hunger, H.; Illy, S.; Jelonnek, J.; Kobarg, T.; Lang, R.; Leonhardt, W.; Losert, M.; Meier, A.; Mellein, D.; Papenfuß, D.; Samartsev, A.; Scherer, T.; Schlaich, A.; Spiess, W.; Thumm, M.; Wadle, S.; Weggen, J. (2019). Impurity transport studies at Wendelstein 7-X by means of x-ray imaging spectrometer measurements. Plasma physics and controlled fusion, 61 (1), Article: 014030.

Livieratos, S.; Ioannidis, Z.; Savaidis, S.; Mitilineos, S.; Stathopoulos, N. (2019). A new prediction method of rain attenuation along millimeter wave links based on a bivariate model for the effective path length and weibull distribution. Progress in electromagnetics research / C, 97, 29–41.

Maksimenko, A. V.; Shcherbinin, V. I.; Hlushchenko, A. V.; Tkachenko, V. I.; Avramidis, K. A.; Jelonnek, J. (2019). Starting Currents for Eigenmodes of a Gyrotron Cavity With Mode Conversion. IEEE transactions on electron devices, 66 (3), 1552–1558.

Pagonakis, I.; Alberti, S.; Avramidis, K. A.; Legrand, F.; Gantenbein, G.; Genoud, J.; Hogge, J.-P.; Illy, S.; Ioannidis, Z. C.; Kalaria, P.; Piosczyk, B.; Ruess, S.; Ruess, T.; Rzesnicki, T.; Tran, M.-Q.; Tran†, T.-M.; Thumm, M.; Vomvoridis, I.; Jelonnek, J. (2019). Overview on recent progress in magnetron injection gun theory and design for high power gyrotrons. The European physical journal / Web of Conferences, 203, 04011.

Peponis, D. V.; Latsas, G. P.; Ioannidis, Z. C.; Tigelis, I. G. (2019). Dispersion properties of rectangularly-corrugated waveguide structures by the in-house 3D FDTD code COCHLEA in cylindrical coordinates. IET microwaves, antennas and propagation, 13 (1), 28–34.

Ruess, T.; Avramidis, K. A.; Gantenbein, G.; Illy, S.; Ioannidis, Z. C.; Jin, J.; Kalaria, P.; Pagonakis, I. G.; Ruess, S.; Rzesnicki, T.; Thumm, M.; Jelonnek, J. (2019). Theoretical Study on the Operation of the EU/KIT TE34,19-Mode Coaxial-Cavity Gyrotron at 170/204/238 GHz. The European physical journal / Web of Conferences, 203, Article no: 04014.

Ruess, T.; Avramidis, K. A.; Gantenbein, G.; Ioannidis, Z.; Illy, S.; Lutz, F.-C.; Marek, A.; Ruess, S.; Rzesnicki, T.; Thumm, M.; Wagner, D.; Weggen, J.; Jelonnek, J. (2019). Computer-Controlled Test System for the Excitation of Very High-Order Modes in Highly Oversized Waveguides. Journal of infrared, millimeter, and terahertz waves, 40 (3), 257–268.

Sanchez, F.; Albajar, F.; Lo Bue, A.; Alberti, S.; Avramidis, K. A.; Bonicelli, T.; Bruschi, A.; Gantenbein, G.; Hogge, J.-P.; Illy, S.; Ioannidis, Z. C.; Leggieri, A.; Legrand, F.; Pagonakis, I.; Perial, E.; Rzesnicki, T.; Thumm, M.; Tigelis, I. (2019). Metrology techniques for the verification of the alignment of the EU gyrotron prototype for ITER. The European physical journal / Web of Conferences, 203, 04015.

Shcherbinin, V. I.; Tkachenko, V. I.; Avramidis, K. A.; Jelonnek, J. (2019). Coaxial Cavity With Stepped Inner Conductor for a Sub-Terahertz Second-Harmonic Gyrotron With Broadband Continuous Frequency Tuning. IEEE transactions on electron devices, 66 (12), 5313–5320.

Thumm, M.; Denisov, G. G.; Sakamoto, K.; Tran, M. Q. (2019). High-power gyrotrons for electron cyclotron heating and current drive. Nuclear fusion.

W7-X Team; Wei, Y.; Wang, E.; Liang, Y.; Brezinsek, S.; Krychowiak, M.; Hammond, K.; Neubauer, O.; König, R.; Sereda, S.; Rudischhauser, L.; Endler, M.; Blackwell, B.; Linsmeier, C.; Gantenbein, G.; Jelonnek, J.; Thumm, M.; Dammertz, G.; Hunger, H.; Illy, S.; Kern, S.; Prinz, O.; Samartsev, A.; Schmid, M. (2019). Spectroscopic studies of fuel recycling and impurity behaviors in the divertor region of Wendelstein 7-X. Plasma science & technology, 21 (10), 105102.

Wilde, F.; Marsen, S.; Stange, T.; Moseev, D. S.; Oosterbeek, J. W.; Laqua, H. P.; Wolf, R. C.; Avramidis, K.; Gantenbein, G.; Pagonakis, I. G.; Illy, S.; Jelonnek, J.; Thumm, M. K. (2019). Automated mode recovery for gyrotrons demonstrated at Wendelstein 7-X. Fusion engineering and design, 148, Art.-Nr.: 111258.

W7-X Team; Wolf, R. C.; Alonso, A.; Äkäslompolo, S.; Baldzuhn, J.; Beurskens, M.; Beidler, C. D.; Biedermann, C.; Bosch, H.-S.; Bozhenkov, S.; Brakel, R.; Braune, H.; Brezinsek, S.; Brunner, K.-J.; Damm, H.; Dinklage, A.; Drewelow, P.; Effenberg, F.; Feng, Y.; Ford, O.; Fuchert, G.; Gao, Y.; Geiger, J.; Grulke, O.; Harder, N.; Hartmann, D.; Helander, P.; Heinemann, B.; Hirsch, M.; Höfel, U.; Hopf, C.; Ida, K.; Isobe, M.; Jakubowski, M. W.; Kazakov, Y. O.; Killer, C.; Klinger, T.; Knauer, J.; König, R.; Krychowiak, M.; Langenberg, A.; Laqua, H. P.; Lazerson, S.; McNeely, P.; Marsen, S.; Marushchenko, N.; Nocentini, R.; Ogawa, K.; Orozco, G.; Osakabe, M.; Otte, M.; Pablant, N.; Pasch, E.; Pavone, A.; Porkolab, M.; Puig Sitjes, A.; Rahbarnia, K.; Riedl, R.; Rust, N.; Scott, E.; Schilling, J.; Schroeder, R.; Stange, T.; von Stechow, A.; Strumberger, E.; Sunn Pedersen, T.; Svensson, J.; Thomson, H.; Turkin, Y.; Vano, L.; Wauters, T.; Wurden, G.; Yoshinuma, M.; Zanini, M.; Zhang, D.; Gantenbein, G.; Huber, M.; Hunger, H.; Illy, S.; Jelonnek, J.; Kobarg, T.; Lang, R.; Leonhardt, W.; Losert, M.; Meier, A.; Mellein, D.; Papenfuß, D.; Samartsev, A.; Scherer, T.; Schlaich, A.; Spiess, W.; Thumm, M.; Wadle, S.; Weggen, J. (2019). Performance of Wendelstein 7-X stellarator plasmas during the first divertor operation phase. Physics of plasmas, 26 (8), Article: 082504.

Wolf, R. C.; Bozhenkov, S.; Dinklage, A.; Fuchert, G.; Kazakov, Y. O.; Laqua, H. P.; Marsen, S.; Marushchenko, N. B.; Stange, T.; Zanini, M.; Abramovic, I.; Alonso, A.; Baldzuhn, J.; Beurskens, M.; Beidler, C. D.; Braune, H.; Brunner, K. J.; Chaudhary, N.; Damm, H.; Drewelow, P.; Gantenbein, G.; Gao, Y.; Geiger, J.; Hirsch, M.; Höfel, U.; Jakubowski, M.; Jelonnek, J.; Jensen, T.; Kasparek, W.; Knauer, J.; Korsholm, S. B.; Langenberg, A.; Lechte, C.; Leipold, F.; Mora, H. T.; Neuner, U.; Nielsen, S. K.; Moseev, D.; Oosterbeek, H.; Pablant, N.; Pasch, E.; Plaum, B.; Pedersen, T. S.; Sitjes, A. P.; Rahbarnia, K.; Rasmussen, J.; Salewski, M.; Schilling, J.; Scott, E.; Stejner, M.; Thomsen, H.; Thumm, M.; Turkin, Y.; Wilde, F. (2019). Electron-cyclotron-resonance heating in Wendelstein 7-X: A versatile heating and current-drive method and a tool for in-depth physics studies. Plasma physics and controlled fusion, 61 (1), Art. Nr.: 014037.

Wu, C.; Pagonakis, I. G.; Albert, D.; Avramidis, K. A.; Gantenbein, G.; Illy, S.; Thumm, M.; Jelonnek, J. (2019). Gyrotron multistage depressed collector based on E × B drift concept using azimuthal electric field. II: Upgraded designs. Physics of plasmas, 26 (1), 013108.

Yuvaraj, S.; Kartikeyan, M. V.; Thumm, M. K. (2019). Design Studies of a 3-MW, Multifrequency (170/204/236 GHz) DEMO Class Triangular Corrugated Coaxial Cavity Gyrotron. IEEE transactions on electron devices, 66 (1), 702–708.

2 Renewable Energy (RE): Bioenergy -Feedstocks and Pretreatment-

Contact: Prof. Dr. Georg Müller

The Department for Pulsed Power Technology is focusing on research and development of pulsed power technologies and related applications. The applications involves the electroporation of biological cells for extraction of cell contents (PEF- process), dewatering and drying of green biomass, pre-treatment of micro algae for energetic use and sustainable reduction of bacteria in contaminated effluents. Another key research topic is devoted to the development of corrosion barriers and materials for improved compatibility of structural materials in contact with liquid metal coolants. This year's report focuses primarily on the activities and results of ongoing third-party funded projects of the department.

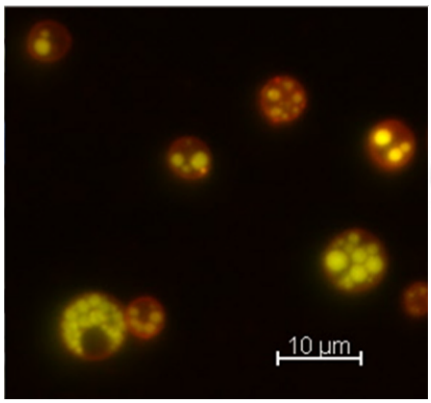

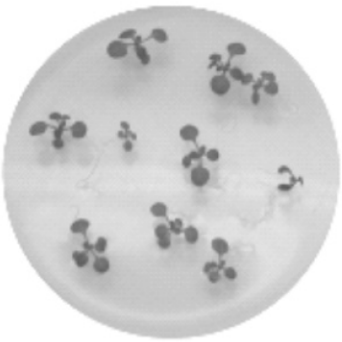

PEF treatment, 10ns pulses

2.1 PEF-Processing of Microalgae and Industrial Water Streams

Contact: Dr. Wolfgang Frey

2.1.1 Extraction of valuable compounds from *Chlorella vulgaris* and *Arthrospira platensis* using PEF treatment

For an economic product recovery from microalgae an efficient cell disruption method as a pretreatment step prior intracellular components extraction is required. In the previous years we have proven that PEF-processing and high pressure homogenization (HPH) are the most appropriate candidates for an economic downstream processing pathway. A main task in the "Research Program on Renewable Energies" is to demonstrate the cascade processing of microalgae biomass by using PEF treatment, i.e. subsequent recovery of several component fractions (lipids, proteins, pigments etc.).

In the course of this research program, we established the microalgae *C. vulgaris* and the cyanobacteria *A. platensis* (known as Spirulina) as model organisms to study the efficiency of PEF treatment on component recovery. Both organisms, which are granted as GRAS (Generally Recognized as Safe), are suitable as an alternative source for proteins with high added value for the production of food and feed. We found in both cases that the release of proteins after PEF treatment is time-dependent and can be influenced by parameters such as biomass concentration, temperature and pH value.

In case of *C. vulgaris* the PEF assisted proteins recovery is mediated by an enzymatically controlled process, induced after cell death. The main conclusion of this work is that protein release is a consequence of cell death and the subsequent autolysis ("self-digestion") of the cell. This process requires an incubation step of several hours and results in maximum yield - if it is carried out under physiological conditions - in a buffered medium with pH of 9 at 30 °C. It could be shown that up to half of the proteins present in the cell can be extracted by PEF treatment and a subsequent incubation step of 8-24 h.

In a second study we investigated how PEF treatment can impact the recovery of proteins and C-Phycocyanin from *A. platensis*. Spirulina is a well-known cyanobacteria due to its high micro and macronutrients synthesis capacity, especially proteins, which could reach up to 70 % of the total cell weight. Phycocyanins, linked to the proteins, are the main pigment found in *A. platensis* and are characterized by a blue color, Fig. 2.1.1. These pigments have shown to exhibit antioxidant activity and can be used in food and pharmaceutical products. Almost the entire amount of phycocyanins and proteins could be recovered by PEF treatment of the Spirulina suspension. In addition, the extracts obtained by PEF treatment exhibit higher antioxidant activity than those obtained by conventional cell disintegration methods. The highest C-Phycocyanin and protein extraction yield were obtained with specific treatment energies of 56 $J \cdot mL^{-1}$ and 112 $J \cdot mL^{-1}$ after 30 min of incubation step. The main advantage of PEF-treatment was the selectivity of extraction of the compounds of interest, producing a more purified extract which could be used in the food and pharmaceutical industries without additional purification techniques.

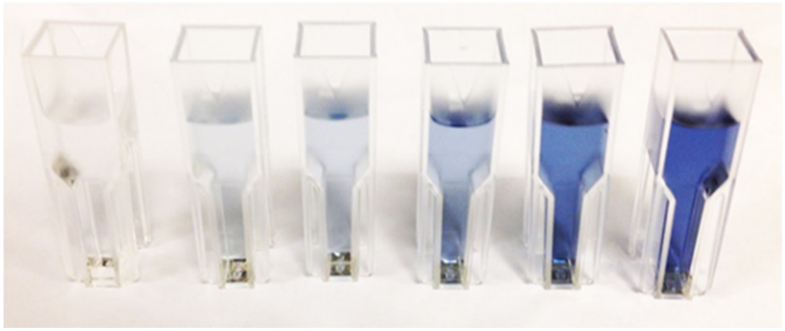

Fig. 2.1.1: Time course of C-Phycocyanin release after PEF treatment. The cuvettes contain the supernatant after separation of the biomass.

These studies show that PEF enables a sequential extraction cascade in which first soluble proteins and then lipids could be extracted by solvent extraction afterwards, all this without the necessity to dry the biomass in between. This would contribute to significant energy savings in processes on an industrial scale and would also fully valorizes the algae biomass.

Collaboration: Federal University of Rio Grande do Sul (UFRGS), Brazil

Funding: Research Program on Renewable Energies - Topic 3: Bioenergy, Helmholtz Gemeinschaft

2.1.2 SABANA-Project: Production of Biofertilizer

One of the objectives of the EU-Project SABANA is to produce amino acid concentrates (biofertilizer) from microalgae biomass. In order to obtain high amounts of amino acids from microalgal proteins through high-yield enzymatic hydrolysis, it is suggested to disrupt the algal cells to liberate proteins. Pulsed electric field (PEF) treatment was suggested as a pre-treatment method prior to enzymatic hydrolysis (Fig. 2.1.2), since it is expected to facilitate enzyme access into the cells in order to cleave intracellular proteins. In addition, released proteins are expected to be hydrolysed easier by enzymes. The influence of PEF treatment on the yield of the enzymatic hydrolysis has been studied in order to assess its potential benefit.

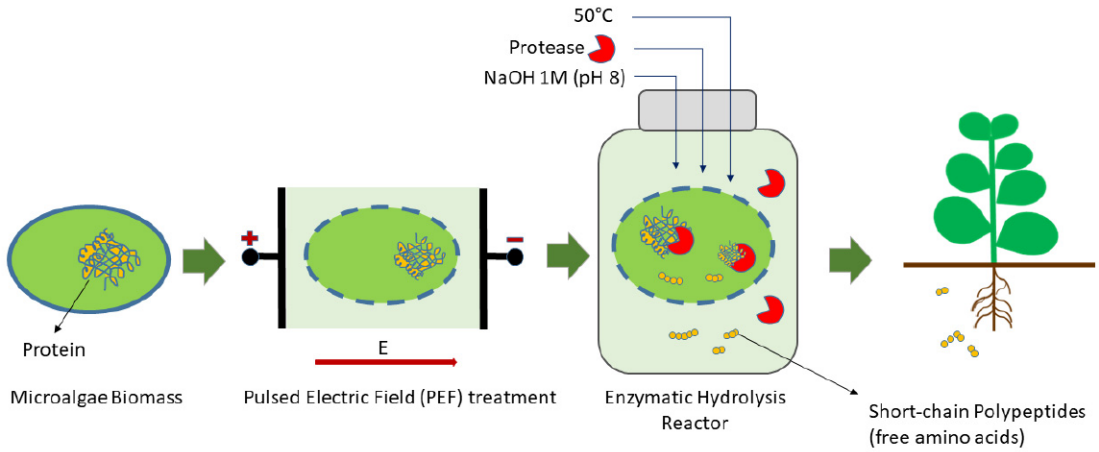

Fig. 2.1.2: Schematic illustration shows pulsed electric field (PEF) treatment as a pre-treatment to fresh microalgae biomass prior to enzymatic hydrolysis to produce amino acids concentrate (biofertilizer).

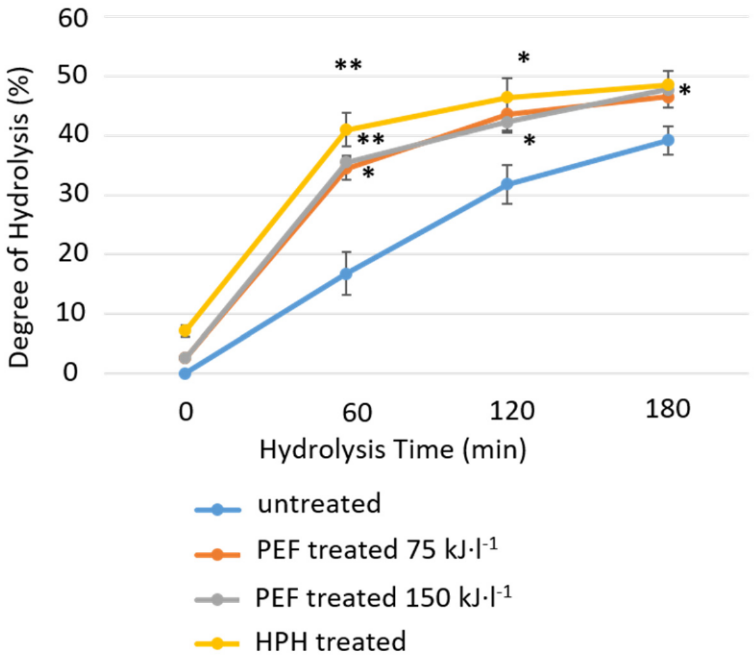

Fig. 2.1.3: Kinetics of the enzymatic hydrolysis of S. almeriensis fresh biomass at 80 $g \cdot l^{-1}$ obtained from PBR after PEF, or HPH treatment using 3% (v·w) enzymes. The experiment was performed in triplicate. Error bars represent standard errors. Asterisks indicate differences that are significant at P = 0.05 (*) or P = 0.01 (**), using a Student's t-test.

The concentrated microalgae suspension (*Scenedesmus almeriensis*) was treated at an initial conductivity of 1 $mS \cdot cm^{-1}$ with 1 µs long pulses at an electric field strength of 40 $kV \cdot cm^{-1}$ and a treatment energy of 150 kJ·l-1 and 75 $kJ \cdot l^{-1}$. For benchmarking, additional biomass samples were processed by high pressure homogenization (HPH).

Hydrolysis kinetics and the final value of the degree of hydrolysis were identical for PEF treatments at an energy input of 150 $kJ \cdot l^{-1}$ and 75 $kJ \cdot l^{-1}$. At a biomass density of 100 $g \cdot l^{-1}$ a PEF treatment energy of 150 $kJ \cdot l^{-1}$ and 75 $kJ \cdot l^{-1}$ correspond to 1.5 $MJ \cdot kg_{dw}$ and 0.75 $MJ \cdot kg_{dw}$. It can be concluded from the hydrolysis results, Fig. 2.1.3, that using the lower energy input of 75 $kJ \cdot l^{-1}$ also leads to adequate permeabilization prior to enzymatic hydrolysis. Our results revealed the advantage of performing PEF at lower energy input along with a high concentration of cells can reduce the energy demand of PEF treatment per kg of dry biomass.

HPH pre-treatment did not exhibit processing advantages over PEF-treatment in terms of the degree of hydrolysis or hydrolysis kinetics. Both pre-treatment methods allow shortening of enzymatic hydrolysis processing time. Based on identical time courses of the degree of hydrolysis for PEF and HPH pre-treatment as well, it can be concluded that membrane permeabilization by PEF enables enzyme entry into the cells and, furthermore, that protein hydrolysis after PEF is as efficient as in the case of free accessible proteins after HPH.

Collaboration: University of Almería, GEA Westfalia, Biorizon

Funding: H2020, SABANA, Grant Agreement No. 727874

2.1.3 DiWaL: PEF-treatment of electrodeposition paints

PEF-treatment was demonstrated to efficiently inactivate bacteria in electrocoating process media. In particular for PEF-treatment of electrodeposition paints, EDP, pulse parameters have to be chosen appropriately that way that EDP does not precipitate at the surface of electrodes of the treatment chamber, potentially resulting in blocking of the chamber. Since paint coagulation and deposition is initiated by electrochemically generated H+ and OH- Ions, EDP deposition at the electrodes' surfaces can be prevented by application of bipolar pulse protocols.

H^+ Ions occurring during the first half-wave of the bipolar pulse will be neutralized by OH^- Ions generated during the second half-wave. As a condition for complete neutralization, the amount of charge during the first half-wave Q^+ has to equal Q^-,

Fig. 2.1.4. Since ohmic heating of the EDP during the first half-wave increases paint conductivity and in consequence pulse current during the second half-wave, pulse duration of the second negative pulse has to be shortened appropriately for fulfilling the condition $|Q^+| = |Q^-|$. This procedure for PEF-treatment of electrodeposition media was disclosed in November 2019.

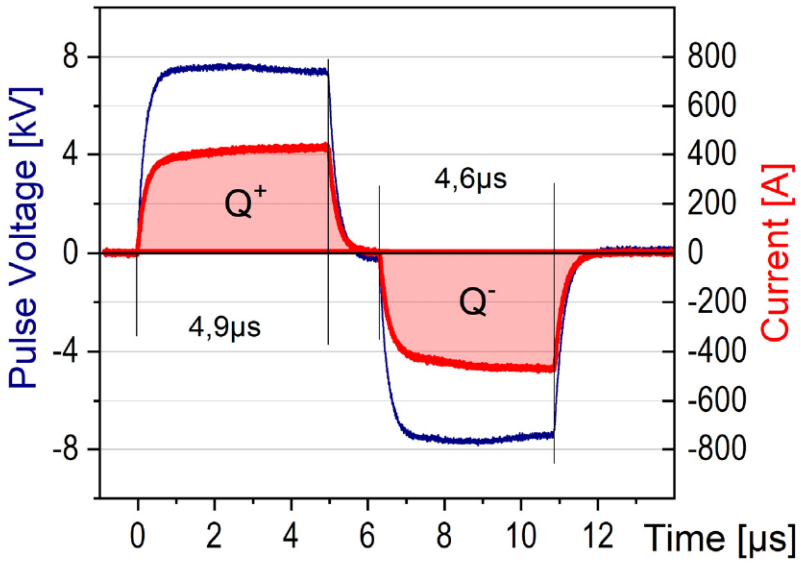

Fig. 2.1.4: Current and voltage waveform for PEF-treatment of electrodeposition paint without precipitation of paint at the surface of the electrodes of the treatment chamber.

2.1.4 Microwave processing of microalgae

In the last two years, the bioelectric group has started a successful collaboration with the microwave department of IHM. The main objective is to explore the effect of pulsed microwave on biological objects and to test the possibility of integrating this new approach in downstream processing of microalgae. Continuous microwave are already routinely used in several extraction process in the field of biotechnology. Transposition to microalgae downstream processing was partially tested with promising results distributed in the literature. According to simulations, we believe that the use of pulsed microwave, as opposed to continuous, can induce higher temperature gradients across cell-wall and therefore induce more cell rupture.

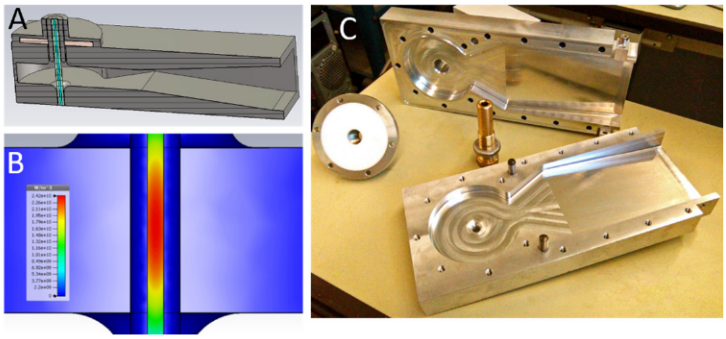

Fig. 2.1.5: A-Cavity cross section. The geometry ensures guiding and then focusing of the microwave on the microalgae suspension contained in a quartz tube at the center of the cavity. B- Simulation of the distribution of the power density inside the cavity showing the focusing of the power inside the microalgae suspension. C- Photos of the various parts of the cavity realized at the mechanical workshop of IHM.

In order to start investigations, the two departments have developed in close collaboration a microwave generator and a TM010 exposure cavity, both custom-designed for the evaluation of microwave disruption of fresh microalgae cells. The generator operates in pulsed mode, delivering pulses of several kilowatt with duration ranging from 1 to 999 µs and repetition rates ranging from 1 to 1000 Hz. The exposure cavity enables exposing a suspension of fresh microalgae biomass suspension to microwave in a continuous flow mode as well as precise monitoring of the microwave energy absorbed by the sample. Fig. 2.1.5 shows a cross section of the cavity (A) and a simulation of the power distribution inside the cavity (B). It can be seen that the power is well focused into the microalgae suspension flowing into a quartz tube located at the center of the cavity. Fig. 2.1.5 (C) shows a photo of the different parts of the cavity manufactured in the workshop of the IHM. This worldwide unique setup is moreover equipped with all necessary sensor to precisely measure the energy absorbed by the microalgae suspension.

First investigations on this new pre-treatment method, performed on model cultivation of *Auxenochlorella protothecoides* were successful with up to 93 % of lipids extracted for energy input not exceeding 2,5 MJ/kg_{DW}. Current investigations are ongoing to optimise the treatment and to compare with continuous microwave approach.

2.1.5 Investigation of PEF impact on stability of microalgae cell wall

Our group has shown in the past how PEF treatment could positively impact lipid extraction using ethanol-hexane blends on the microalgae *Auxenochlorella protothecoides.* Lipid yields could reach up to 40 % (dry weight) after treatment in contrast to untreated control samples for which lipid yield typically did not exceed 5 % (dry weight). Reasons for such an inhencement are still not understood. The dramatic consequences of PEF treatment on cell membrane of *A. Protothecoides* that have been observed and reported in the past are unlikely to explain alone the enhancement of lipid yield. In an attempt to better understand the PEF-treatment effect, experiments were conducted to analyse modification of the cell wall. High pressure homogenisation was used as a diagnostics to quantify the mechanical stability of cell wall and to measure a possible impact of PEF-treatment. Experiements performed on *A. protothecoides* cultivated in two modes (mixotrophically and autotrophically) and on *C. vulgaris* suggest no impact of the PEF-treatment of mechanical stability of the microalgae under test. Scanning electron microscopy imaging allowed for an external examination of the cells and showed no modification of the outside layer of cell wall. Further investigations are currently ongoing in order to evaluate if chemical composition of the cell-wall is affected by PEF-treatment.

2.1.6 Biogas production from residuals from microalgae biorefinery

PEF-processing, which enables the economic utilization of residuals from already processed microalgae, fosters the improvement of the microalgal value chain significantly. Anaerobic digestion (AD) of microalgal residues by anaerobic microorganisms, for biogas production, exhibits promising potential for that purpose. Biogas has the advantage to be an easy storable form of energy, which can be distributed by feeding into the existing natural gas grid.

For an efficient production of biogas, or rather bio-methane, from microalgae, access to ingredients of microalgal cells for more effective AD is highly desirable. In particular, a better access of AD-performing microorganisms to digestible biomolecules is advantageous. Faster kinetics of AD processes and an increased yield can be expected.

Basically, supernatants from four differently treated microalgae (*Auxenochlorella protothecoides*) biomass samples (DCW≈100g_{DCM}/kg_{susp}) were selected for analysis: 1. untreated biomass, i.e. just harvested, 2. PEF-treated, 3. PEF-treated and with subsequent replacement of supernatant by deionized water after centrifugation, at six different waiting times and 4. aqueous eluate of PEF-treated and lipid-extracted samples. The investigation refers to two different observation periods. The first set of samples was examined on the same day of experiment as shown in Fig. 2.1.6, left. The second set, consisting of duplicates of the first set, was examined 20 days after the corresponding experiment, stored in the fridge, at T=9°C, meanwhile as shown in Fig. 2.1.6, right. By applying this approach, we took into account that microalgae residues will most likely not be processed in an AD-plant, directly after PEF-treatment. With regard to storage, handling and transportation of the microalgal residues from preceeding value-added processes, a specified waiting time appeared reasonable. In this way we included the impact of disintegration of microalgal cells, on the release of non-extracted ingredients and liberation of digestible components of the cells´ structural components (e.g. bio membranes, cell-wall).

Compared to harvested and untreated microalgae (grey), PEF-treated microalgae (red) display a large increase of liberated ions and molecules, as expected. Especially noticeable is the release of sulfur (+3.315%). Even PEF-treated microalgae with supernatants, replaced by deionized water, at delays of 0 to 150 minutes (shades of yellow) show a significant further release of monitored species. Surprisingly high was the content of TOC in the aqueous eluate of PEF-treated and lipid-extracted microalgae (+450 %) (cyan), related to the state of harvest (grey). As TOC-content can be set in relation to biogas-production, an extra gain of bio methane in addition to the already extracted lipids can be expected.

In principal, with 20 days delay, most observed species are available in appreciably higher concentrations, than obtained on day of experiment. Remarkable is the strong increase of released phosphate-ions (+944%) of PEF-treated samples. Expenses for micro nurtients like phosphate contribute significantly to cultivation cost. This may cause higher expenditures for any product in the subsequent exploitation chain. For that reason it should be noticed that PEF-assisted cultivation media recycling could be a valuable contribution on economic and ecological usage of microalgae.

Especially the noticeable increase in TOC-externalization (harvest: +84 %, just PEF-treated: +79 %, PEF-treated + lipid-extracted: +23 %) during the waiting time, rises the expectation of an increased bio-methane production. Only the liberation of small amounts of ammonium ions, a well-known inhibitor in AD process, after 20 days delay, is unwanted. In view of the small amount of this liberated species, inhibitory effects on the AD process are unlikely, regarding information from the literature, though.

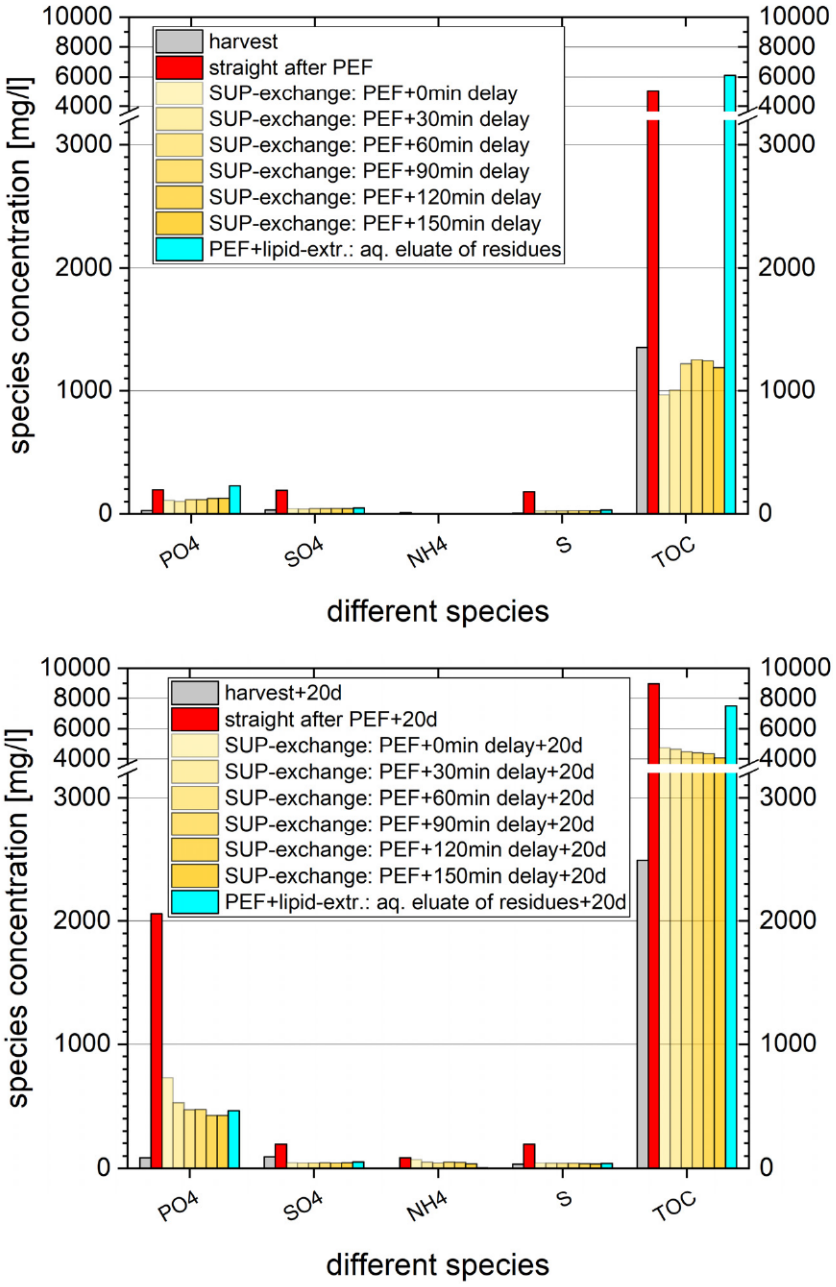

Fig. 2.1.6: Concentration of substances in supernatants from PEF-treated microalgae biomass for different incubation times (delay) after PEF-treatment, for untreated biomass (harvest) and for PEF-treated biomass after lipid extraction, analyzed on day of the experiment, top, and analyzed 20 days after the experiment, bottom.

Sulfur, another important micronutrient for growth of methanogenic microorganisms exists in rather high concentrations. With c_S~30-200 mg/L, present alone in the supernatant, the concentration is clear above $c_{S\text{-}optimal}$=1-25 mg/L, mentioned in literature. In anaerobic reactors sulfate is reduced to sulfide by sulfate reducing bacteria (SRB). Sulfides are toxic for methanogenic bacteria in the form of H_2S, in doses at c_{H2S}=50- 125mg/L. An inhibitive effect on methan production might arise from sulfur- and SO_4-fraction, hence.

Considering all results of this investigation, the approach of an approximately three week-delay after harvest, before the usage of microalgae residues as substrate for AD, appears advantageous, hence.

2.2 Components and electroporation processes

Contact: PD Dr. Martin Sack

2.2.1 ZIM-Wine

In the frame of the joint research project "PEF-treatment of crushed grapes (Elektroporation von Traubenmaische)" a device for the treatment of crushed grapes by pulsed electric fields (PEF) with a flow rate of 10 t/h is currently being developed in collaboration with the industrial partners ARMBRUSTER Keltereitechnologie and KEA-TEC. The project is supported by the Federal Ministry for Economic Affairs and Energy on the basis of a decision by the German Bundestag.

In 2019 the electroporation device has been put into operation and tested successfully. In autumn crushed grapes of the grape varieties Pinot Noir and Riesling have been processed. Fig. 2.2.1 shows the electroporation device with its feeder pump in the foreground. The feeder pump pressurizes the mash to approximately 0.2 MPa above ambient pressure and feeds it via a hose to the device. A second pump near the device's outlet lowers the pressure back to ambient pressure. Fig. 2.2.1 also shows the mash just leaving the device. The extraction of pigments and valuable substances starts just after the processing.

Fig. 2.2.1: Electroporation device with its feeder pump (left) and mash leaving the device (right).

Collaboration: ARMBRUSTER Keltereitechnologie, KEA-TEC

Funding: The project is supported by the Federal Ministry for Economic Affairs and Energy on the basis of a decision by the German Bundestag.

ZIM Zentrales Innovationsprogramm Mittelstand

Supported by: Federal Ministry for Economic Affairs and Energy on the basis of a decision by the German Bundestag

2.2.2 Semiconductor-based Marx-type Pulse Generator for PEF-treatment of Root Vegetables

For the PEF-treatment of root vegetables in industrial scale a Marx-type pulse generator equipped with IGBT switches is currently being developed. For an energy-efficient operation of the pulse generator the pulse switches are operated under soft-switching conditions. Fig. 2.2.2 shows voltage and current measured at the output of one stage connected to a combined resistive and inductive test load. Switching occurs always under zero-current conditions. The stage comprises a pulse capacitor and an IGBT switch together with a bypass diode and is equipped with a microcontroller. The microcontroller controls the pulse generation locally at the stage when receiving a trigger signal from a main control unit and provides sensor signals back to the main control unit via a fiber-optic link. An auxiliary power supply provides power at low voltage to the stage's control circuitry. It is powered from the pulse capacitor's charging voltage and is operative within a stage voltage range between approximately 50 V and the rated stage voltage of 1 kV. The stage has been designed for a pulse current of up to 500 A and a pulse length in the range of t_h = 10 µs. In the course of first tests it has been operated successfully at its rated pulse repetition rate of 500 Hz resulting in an average power of 1.5 kW supplied to the load. During the tests, cooling by means of ambient air without ventilation was sufficient to keep the operating temperature of the device within acceptable limits.

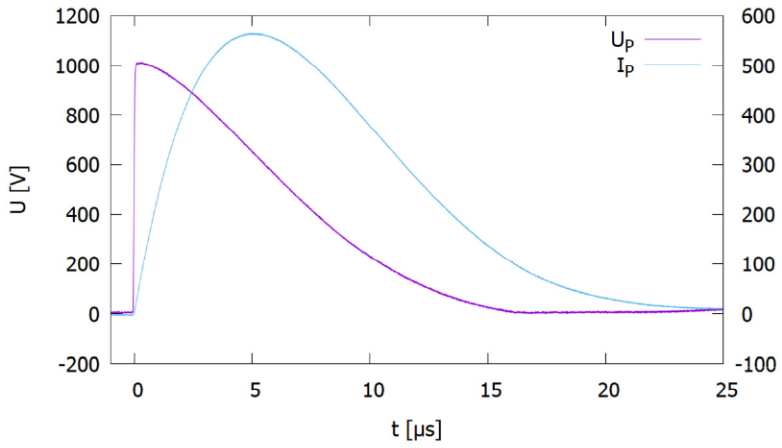

Fig. 2.2.2: Voltage and current at the output of one stage under test.

2.2.3 Marx-type Pulse Generator for PEF-treatment of Paint

In the frame of the DiWaL-project dealing with the PEF-treatment of electrodeposition paint and process water for decontamination purpose, an 8-stage pulse generator for the generation of rectangular bipolar ground-symmetric pulses in the microsecond range has been applied successfully for laboratory-scale experiments on the PEF-treatment of paint. Crucial for the experiment was the application of an AC current to the electrode system without a considerable DC offset to prevent the paint from coating the electrodes.

The pulse generator is equipped with IGBT switches in H-bridge configuration. In order to protect the switches against over-current in case of a flashover inside the PEF treatment chamber, a fast overcurrent protection circuitry has been developed. Fig. 2.2.3 shows the current at the output of a shorted generator stage operated at varying stage voltage. Detection of an overcurrent condition and current limitation both are achieved within less than 100 ns. Thereby, the current rises up to 1.5 kA, which is still within the design limits of the switch under transient conditions.

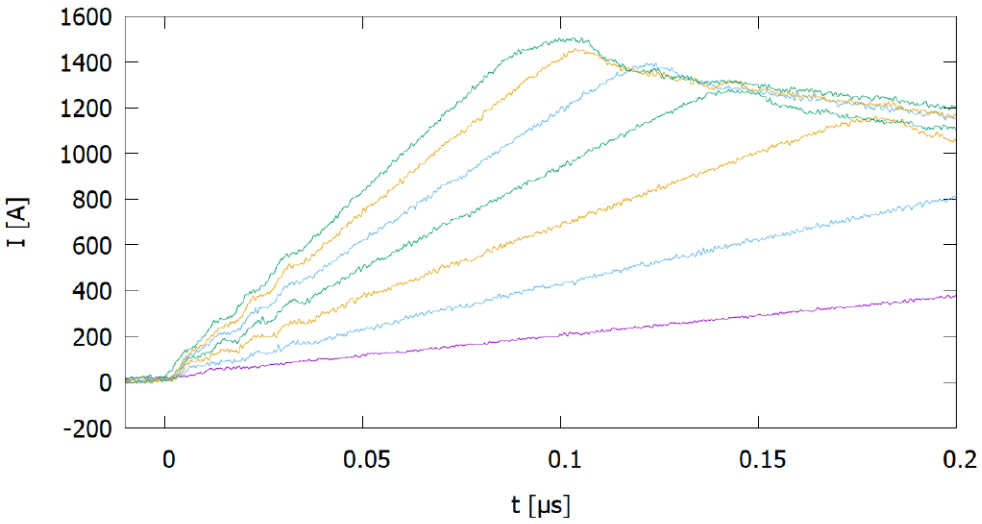

Fig. 2.2.3: Overcurrent protection: Output current of a shorted stage operated at varying stage voltage.

Based on the stage design of the 8-stage generator used for the laboratory-scale tests, a 30-stage pulse generator is currently being assembled and tested. It consists of two stacks of 15 stages each. Fig. 2.2.4 shows both stacks mounted inside a shielded enclosure.

Fig. 2.2.4: 30-stage bipolar pulse generator: Two stacks of 15 stages each mounted inside a shielded enclosure.

2.3 Concentrating solar power (CSP)/ Liquid metal

– Material research – improving the compatibility of materials for CSP

Contact: Dr. Alfons Weisenburger

Liquid metals as advanced heat-transfer media (HTM) and storage media for CSP are a promising research area that will result in performance and efficiency increase and reduced costs. Within LIMCKA (Liquid Metal Competence Center KArlsruhe) several institutes and laboratories of the KIT combine their long-standing experience and specific expertise in material research, system engineering, safety and thermal-hydraulics to tackle all relevant aspects of liquid metals as HTM. The IHM focuses on compatibility research by surface optimization of existing materials using GESA and development of new materials that are able to mitigate corrosion in contact with liquid metals and salts. Liquid metal batteries are a new research area where the expertise of the IHM and DLR is combined with the expertise of a Chinese university (HUST) to explore Sb- Bi (Sn)/ Na based low cost liquid metal battery concepts in the frame of a German-Chinese DFG project.

Some of the tasks are embedded in European projects, the EERA-CSP and cooperations like with DLR and HUST via DFG.

2.3.1 GESA – SOFIE

Contact: DP Wladimir An

The well-established GESA-concept applying a converging beam guidance does not allow an increase of the current density above 2-3 A/cm² for pulse durations longer than 200 µs. This limitation results from the limited emission of the multipoint explosive emission cathode and the low mirror coefficient and represents therefore a general limit. Nevertheless, this concept is still usable in a wide area of applications due to its stability and robustness.

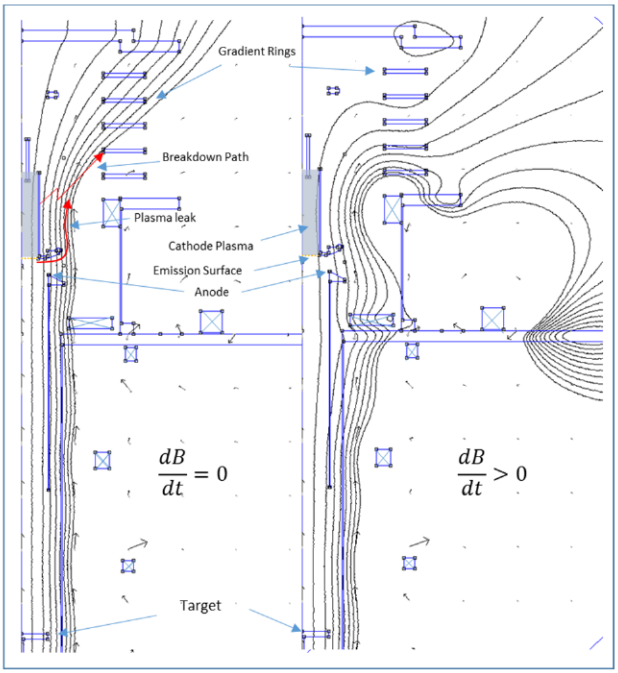

Fig. 2.3.1: Magnetic flux distribution for constant and increasing flux suppressing cathode plasma expansion.

To overcome the limit regarding duration and current density, the design of a new type of cathode with a compression free beam guidance was realized and implemented in the GESA-Sofie.

A hollow cathode with stabilizing grid as electron source allows an order of magnitude higher current densities. This opens the possibility of operate the GESA without a converging beam guidance that is associated with issues like beam precession, losses in the transport area, and fluctuations in the beam profile. Already in the first testing phase, current densities of 3 A/cm² with pulse durations of up to 500 ms were achieved.

One problem of the new configuration is the much stronger influence of the magnetic field on the emission plasma. Stable operation without excessive plasma generation and non-controlled expansion requires a careful configuration of the magnetic field, adapted to the real electrode geometry. A stationary magnetic field seems not to be the best option. A ballistic beam guidance without magnetic field is an alternative operation mode for shorter pulses (<100 µs) and moderate current densities (up to 2 A/cm²).

2.3.2 Material development

Dr. Adrian Jianu, Dr. Alfons Weisenburger

The focus on material development was on alumina-forming high entropy alloys (HEA) and alumina-forming austenitic (AFA) steels and FeCrAl in contact with all liquid metals of interest (Sn, Na, Pb and Sb-Bi/Sn alloys) and solar salts. The material selection for the liquid metal battery project was started by testing several ferritic and austenitic steels, Mo, Cr and three MAX phase coatings in liquid Sb-Bi and Sb-Sn. As test temperature 450 °C was selected, which is the upper limit of the targeted temperature ranges for the selected LM battery concept. Both tests were performed at reducing conditions for a duration of 750 h. Beside Mo and the three MAX phase coatings all other materials showed more or less strong dissolution attack. None of the steels can be employed at 750 °C without further protection.

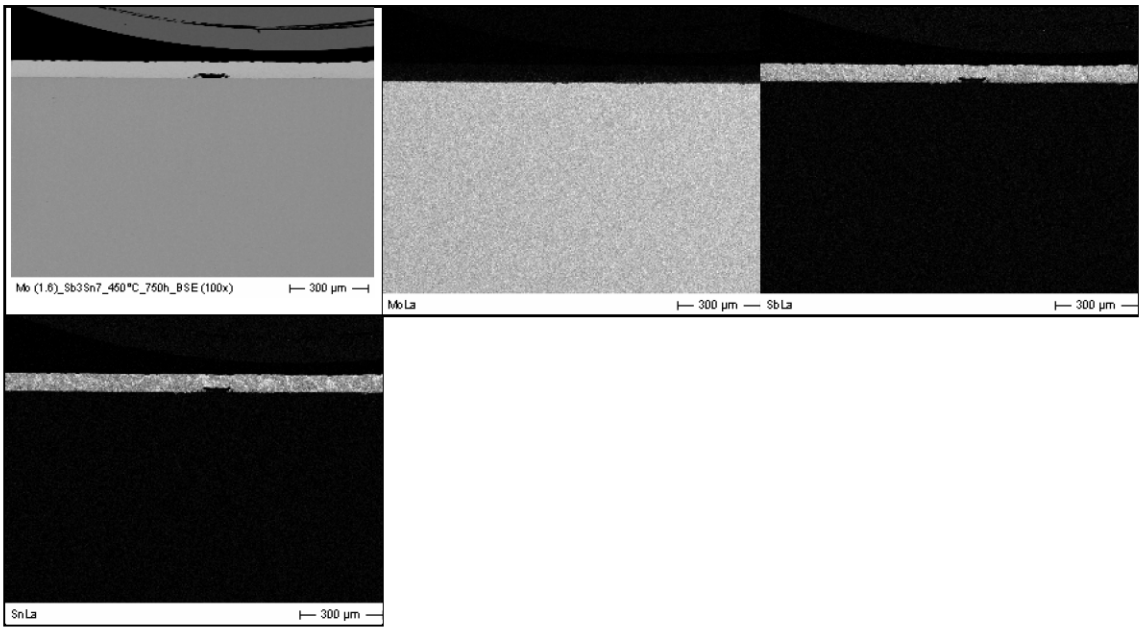

Fig. 2.3.2: x2 Scanning electron microscopy of a cross section (upper left) and elemental mapping (Mo, Sb, Sn from the left) of Mo sample after exposure to Sb3Sn7 at 450 °C for 750 h.

Involved Staff:

Dr. S. Akaberi, W. An, K. Baumann, Dr. R. Fetzer, J. Fleig, **Dr. W. Frey**, Dr. Ch. Gusbeth, Dr. A. Heinzel, D. Herzog, Dr. M. Hochberg, Dr. A. Jianu, D. Krust, F. Lindner, F. Lang, K. Leber, Dr. G. Link, **Prof. G. Müller**, N. Nazarova, I. Papachristou, J. Ruf, **PD Dr. M. Sack**, Dr. D. Scherer, Dr. G. Schumacher (Guest), Dr. H. Shi, Dr. A. Silve, A. Sivkovich, Dr. S. Soldatov, DI R. Sträßner, Z. Wang (CSC-PhD student), **Dr. A. Weisenburger**, R. Wüstner, Y. Zhang, T. Zhang (DFG-PhD student)

Journal Publications

Akaberi, S.; Gusbeth, C.; Silve, A.; Senthilnathan, D. S.; Navarro-López, E.; Molina-Grima, E.; Müller, G.; Frey, W. (2019). Effect of pulsed electric field treatment on enzymatic hydrolysis of proteins of Scenedesmus almeriens. Algal Research, 43, 101656.

Buchmann, L.; Frey, W.; Gusbeth, C.; Ravaynia, P. S.; Mathys, A. (2019). Effect of nanosecond pulsed electric field treatment on cell proliferation of microalgae. Bioresource technology, 271, 402–408.

Guo, B.; Yang, B.; Silve, A.; Akaberi, S.; Scherer, D.; Papachristou, I.; Frey, W.; Hornung, U.; Dahmen, N. (2019). Hydrothermal liquefaction of residual microalgae biomass after pulsed electric field-assisted valuables extraction. Algal Research, 43, 101650.

Jaeschke, D. P.; Mercali, G. D.; Marczak, L. D. F.; Müller, G.; Frey, W.; Gusbeth, C. (2019). Extraction of valuable compounds from Arthrospira platensis using pulsed electric field treatment. Bioresource technology, 283, 207–212.

Polikovsky, M.; Fernand, F.; Sack, M.; Frey, W.; Müller, G.; Golberg, A. (2019). In silico food allergenic risk evaluation of proteins extracted from macroalgae Ulva sp. with pulsed electric fields. Food chemistry, 276, 735–744.

Scherer, D.; Krust, D.; Frey, W.; Müller, G.; Nick, P.; Gusbeth, C. (2019). Pulsed electric field (PEF)-assisted protein recovery from Chlorella vulgaris is mediated by an enzymatic process after cell death. Algal Research, 41, Article no: 101536.

Shi, H.; Jianu, A.; Weisenburger, A.; Tang, C.; Heinzel, A.; Fetzer, R.; Lang, F.; Stieglitz, R.; Müller, G. (2019). Corrosion resistance and microstructural stability of austenitic Fe–Cr–Al–Ni model alloys exposed to oxygen-containing molten lead. Journal of nuclear materials, 524, 177–190.

Tyerman, S. D.; Munns, R.; Fricke, W.; Arsova, B.; Barkla, B. J.; Bose, J.; Bramley, H.; Byrt, C.; Chen, Z.; Colmer, T. D.; Cuin, T.; Day, D. A.; Foster, K.; Gilliham, M.; Henderson, S. W.; Horie, T.; Jenkins, C. L. D.; Kaiser, B. N.; Katsuhara, M.; Plett, D.; Miklavcic, S. J.; Roy, S. J.; Rubio, F.; Shabala, S.; Shelden, M.; Soole, K.; Taylor, N. L.; Tester, M.; Watt, M.; Wege, S.; Wegner, L. H.; Wen, Z. (2019). Energy costs of salinity tolerance in crop plants. The new phytologist, 221 (1), 25–29.

3 Safety Research for Nuclear Reactors (NUSAFE): Transmutation -Liquid Metal Technology-

Contact: Prof. Georg Müller

Long-living high-level radioactive waste from existing nuclear power reactors should be transmuted in short-living radio nuclides using fast neutrons provided by a spallation target in an accelerator driven subcritical system or by a fast nuclear reactor. The objective is to reduce the final disposal time of high-level radioactive waste (plutonium, minor actinides) from some 10^6 years down to about 1000 years. Lead (Pb) and lead-bismuth (PbBi) are foreseen as spallation-target and coolant of such devices.

The aim of the institute's contribution is to develop advanced corrosion mitigation processes based on in-situ formation of protective alumina scales especially for parts under high loads like fuel claddings or pump materials in contact with liquid Pb or PbBi. Pulsed large area electron beams (GESA) are used to create aluminum containing surface alloys on steels. In addition, bulk alumina formers like FeCrAl, AFA (alumina forming austenitic steels) and HEA (high entropy alloys) are developed.

All tasks are embedded in European and international projects and cooperations like e.g., ILTROVATORE, MYRTE, GEMMA and EERA-JPNM.

The most relevant results obtained in the reporting period are presented briefly:

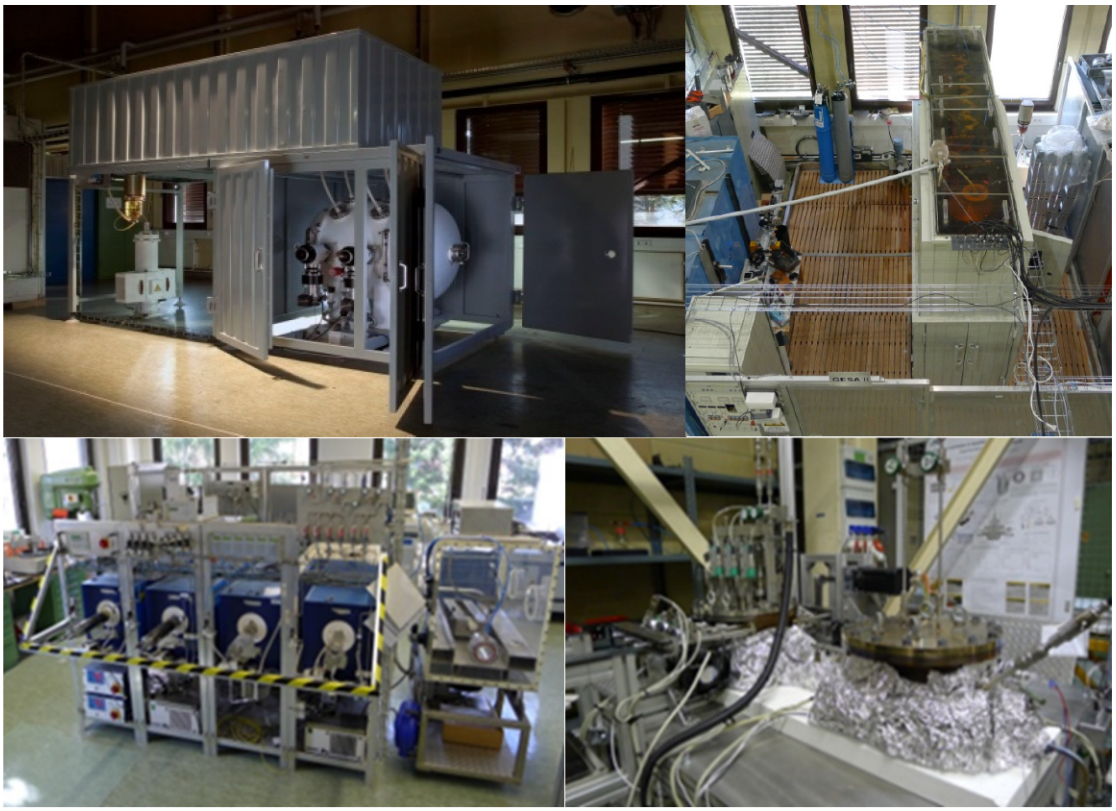

3.1 Material development and advanced corrosion mitigation strategies for heavy liquid metal-cooled nuclear systems

Contact: Dr. Alfons Weisenburger

3.1.1 Simulations of oxygen transport in the COSTA facility

Contact: Dr. Renate Fetzer

Investigation of corrosion/oxidation in oxygen-containing liquid metals is performed either in flowing or in stagnant conditions. One of the facilities routinely used for experiments in stagnant liquid metals is the COSTA facility at IHM. The liquid metal (lead or lead-bismuth eutectic) is placed inside an open alumina crucible. By controlling the oxygen partial pressure in the gas stream above the crucible, oxygen is transferred across the free liquid metal surface until the oxygen concentration in the liquid metal reaches equilibrium with the oxygen partial pressure in the gas stream above (same oxygen potential). Once a specimen is placed inside the liquid metal under oxidizing conditions, the oxygen dissolved in the liquid metal is consumed at the specimen surface by oxidation. In order to provide stationary conditions and to maintain the oxidation process, sufficient oxygen supply from the gas phase via the liquid metal to the specimen surface needs to be ensured. Although experiments performed for many years clearly demonstrate sufficiently high oxygen transport through the liquid metal, the exact explanation is still lacking. The problem is that diffusion alone is not fast enough (by about two orders of magnitude) to provide the required oxygen transport. In the reporting period, therefore, the oxygen transport inside the liquid metal was studied for the arrangement in the COSTA facility. From the temperature distribution inside the oven and the gas stream, a temperature drop of about 0.2 K between the crucible bottom and the upper edges was estimated, which leads to natural convection and Marangoni-driven flow. The combination of oxygen diffusion and oxygen convection due to thermo-capillary flow is able to provide sufficient oxygen transport from the liquid metal free surface to the specimen surface.

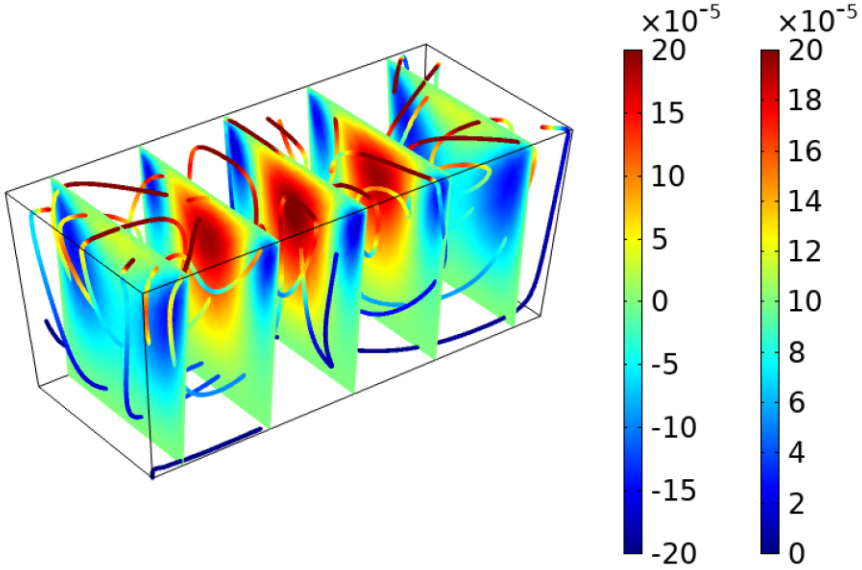

Fig. 3.1.1: Thermo-capillary flow of liquid lead for a temperature drop of 0.1 K. Colour of surfaces shows vertical velocity component (left scale bar), colour of streamlines shows velocity magnitude (right scale bar).

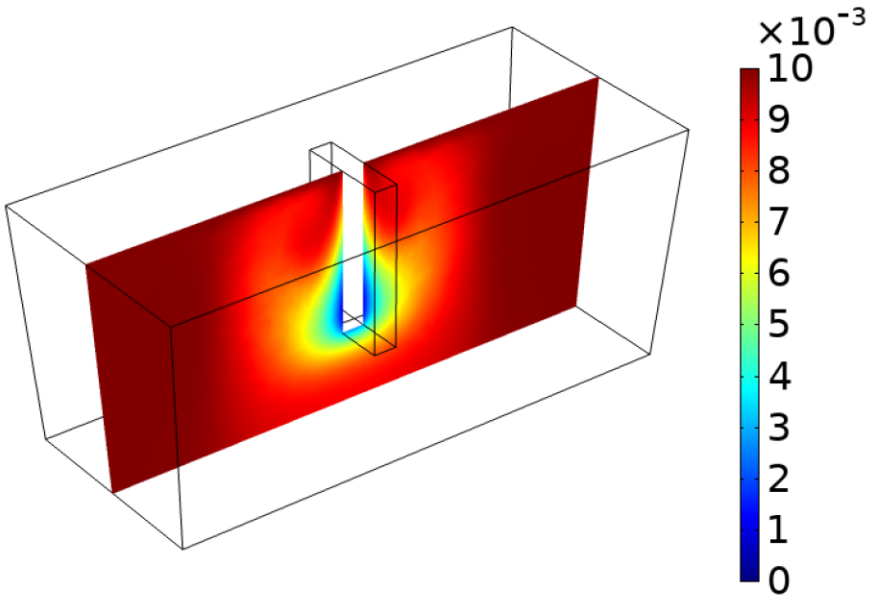

Fig. 3.1.2: Stationary oxygen concentration (in mol/m³) for a typical oxide scale growth rate of 1 µm per 1000 h and an oxygen concentration of 0.01 mol/m³ at the free surface (corresponds to $1.6 \cdot 10^{-6}$ wt%).

3.1.2 Material development to mitigate corrosion

Contact: Dr. Annette Heinzel, Dr. Adrian Jianu, Dr. Alfons Weisenburger

Within the EU Project GEMMA a round robin test with AISI 316L steel was conducted. In the COSTA facility specimens were exposed for 1000 h at 550 °C in Pb and at 500 °C in LBE. For each liquid metal, one test was performed at reducing conditions and two tests were performed with a target oxygen content of 10^{-6} wt% based on two different equations of the oxygen saturation data (OECD Handbook on Lead-bismuth Eutectic Alloy and Lead Properties and published data IHM, KIT). To distinguish between both tests, the oxygen concentration in wt% is given using the saturation correlation of the OECD handbook. Tests at reducing conditions were additionally performed in a corrosion capsule dedicated for the EU MATTER project in LBE at 500°C. All the specimens exposed had one polished and one machined side.

As expected, at 500 °C in oxygen containing PbBi ($1x10^{-6}$ and $5x10^{-6}$ wt% O), a layered oxide of about 4.5 µm thickness consisting of magnetite and spinel was formed on the polished surface. The only visible difference is the size of the oxide roots underneath the scale (8 to 9 µm at $1x10^{-6}$ wt% O compared to 12 µm at $5x10^{-6}$ wt% O). The just machined sides of both samples were protected by a very thin oxide scale. At 550 °C with $1x10^{-6}$ wt% O in Pb the oxide scale grows on the polished side faster to a thickness of 13.6 µm (magnetite +spinel) with roots of maximum length of 28 µm. A slight decrease in oxygen content in the liquid metal to $5x10^{-7}$ wt% O resulted in Cr-Fe oxides with Pb inclusions and dissolutions attack (Fig. 3.1.3). A mixture of a thin Cr-Fe-O with dissolution attack was observed at the machined sides exposed to Pb with 10^{-6} wt% O, while at $5x10^{-7}$ wt% O a 1.3 µm thick Cr-rich Fe-oxide protected the surface.

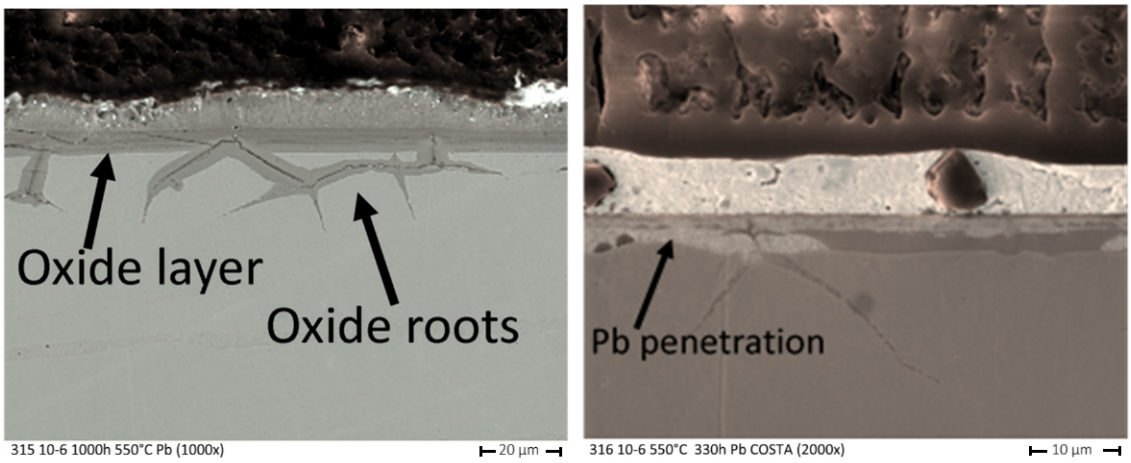

Fig. 3.1.3: Comparison between AISI316L exposed 1000 h to Pb at 550 °C with 10^{-6} wt% O (left side) and $5*10^{-7}$ wt% O (right side).

All specimens in reducing environment exhibit the well-known dissolution attack. The maximum attack in LBE at 500 °C was 10.5 µm (polished side) and13.5 µm (machined side), in Pb at 550 °C the maximum attack reaches 73 µm at the polished side and 43 µm at the just machined side. In the case of the capsule test, the maximum depth was 51.4 µm (10^{-9}-10^{-5} wt% O) and 12 µm (below $5x10^{-12}$ wt% O).

Bulk alumina formers like (AFA and alumina forming HEA alloys), which are designed and manufactured at the IHM are tested regarding their compatibility with liquid metals and other properties. The thermal conductivity and linear expansion coefficient of all produced AFA alloys was in the range of the austenitic steel 316. Together with SANDVIK, an industrial partner in the GEMMA project, four AFA steels with different Al content were produced in the kg range. These steels showed good corrosion resistance up to 750 °C and will be explored further regarding their mechanical properties and irradiation stability.

Three AFA and four aluminum containing HEA alloys were tested in steam at a temperature of 1200 °C. AFA model alloys with the composition Fe-3Al-16Cr-(19-21)Ni (wt.%) show an excellent oxidation resistance to steam by forming external α-Al_2O_3 scale at 1200 °C. With yttrium addition, the scale adherence is improved and in consequence, the scale exfoliation phenomenon is avoided. HEAs with the formula Al(7.9-8.9)Cr(21.4-23.2)Ni(34.3-35)Fe bal. (at.%) form an α-Al_2O_3 scale during exposure to steam at 1200 °C. By adding Nb, the scale adherence has been improved in terms of reduced scale exfoliation compared to HEA alloys without Nb. Adding Ti degrades the oxidation resistance of HEA alloy due to the formation of less protective TiO_2 and Fe_3O_4 layers, leading to an extended internal oxidation.

Collaboration: SCK-CEN, ENEA, KTH, SANDIVK, CIEMAT, CEA

Funding: EU-Projects and NUSAFE

Involved Staff

Dr. DP W. An, Dr. R. Fetzer, Dr. A. Heinzel, Dr. A. Jianu, F. Lang, F. Lindner, Prof. G. Müller, Dr. G. Schumacher (Gast), Dr. H. Shi, A. Sivkovich, **Dr. A. Weisenburger**, Z. Wang (CSC-PhD student)

Journal Publications

Ding, W.; Shi, H.; Jianu, A.; Xiu, Y.; Bonk, A.; Weisenburger, A.; Bauer, T. (2019). Molten chloride salts for next generation concentrated solar power plants: Mitigation strategies against corrosion of structural materials. Solar energy materials & solar cells, 193, 298–313.

Engelko, V. I.; Fetzer, R.; Tkachenko, K.; Shchegolikhin, K.; Müller, G. (2019). Experimental Study of the Accelerator of a Pulsed High-Current Radially Converging Electron Beam. IEEE transactions on plasma science, 47 (1), 329–335.

Fetzer, R.; Müller, G. (2019). Numerical Study of Circulating Electrons in a Cylindrical Accelerator With Converging Electron Beam. IEEE transactions on plasma science, 47 (2), 1290–1296.

Geanta, V.; Voiculescu, I.; Stefanoiu, R.; Jianu, A.; Milosan, I.; Stanciu, E. M.; Pascu, A.; Vasile, I. M. (2019). Titanium influence on the microstructure of fecral alloys used for 4R generation nuclear power plants. Revista de chimie, 70 (2), 549–554.

Hochberg, M.; Sack, M.; Herzog, D.; Weisenburger, A.; An, W.; Fetzer, R.; Müller, G. (2019). A Fast Modular Semiconductor-Based Marx Generator for Driving Dynamic Loads. IEEE transactions on plasma science, 47 (1), 627–634.

Lapauw, T.; Tunca, B.; Joris, J.; Jianu, A.; Fetzer, R.; Weisenburger, A.; Vleugels, J.; Lambrinou, K. (2019). Interaction of Mn+1AXn phases with oxygen-poor, static and fast-flowing liquid lead-bismuth eutectic. Journal of nuclear materials, 520, 258–272.

Loisch, G.; Engel, J.; Gross, M.; Hochberg, M.; Huck, H.; Koss, G.; Lishilin, O.; Oppelt, A.; Philipp, S.; Richter, D.; Stephan, F.; Weidemann, P. (2019). Jitter mitigation in low density discharge plasma cells for wakefield accelerators. Journal of applied physics, 125 (6), Art.Nr.: 063301.

4 Energy Efficiency, Materials and Resources (EMR): Energy-Efficient Processes -Multiphases and thermal processes-

Contact: Dr. Guido Link

Besides the activities on development of technologies and systems for the plasma heating in the FUSION Program, IHM is also in charge of research and development in the topic Energy Efficient Processes, part of the EMR Program.

An important part of this research is the dielectric characterization of the processed materials in the parameter range relevant to processes under development. Therefore existing test-sets are continuously improved and new test-set are developed following the new requirements regarding materials compositions or process parameter range. Meanwhile a very versatile test lab for dielectric characterization exists. This allows temperature dependent dielectric measurements in the frequency range from 10 MHz to 30 GHz for low as well as high loss materials and from room temperature up to 1000°C for solids, liquids and at pressures up to 20 bar.

All this expertise and the existing industrial scale high power microwave infrastructure faces growing interest from industry and research. As a consequence the research group is involved in several national and international joint research projects with objectives in various fields of applications. In the frame of the EU Horizon 2020 Marie Curie international training network TOMOCON a microwave tomographic sensor is under development and is planned to be used to control of a microwave assisted drying process. Within the German-Korean project REINFORCE the potential of microwave dielectric heating has been investigated with respect to energy efficient carbon fiber production. The national funded joint project e-KOMFORT, coordinated by KIT investigates the microwave assisted and energy efficient lamination of synthetic leather for automotive industry. Another national project IMPULS develops an innovative microwave applicator for the microwave assisted intermittent pultrusion of CFRP profiles. In the frame of an AvH fellowship and innovative technology for microwave assisted 3D printing of continuous carbon fiber reinforced polymers has been developed and successfully demonstrate.

Solid state microwave amplifiers getting more and more competitive compared to magnetron sources with respect to power and costs. Furthermore such amplifiers allow precise control not only of power level but also of frequency and phase and promise significant longer lifetime than magnetrons. Those features and novel process control concepts might be door openers for novel application that could not be satisfied with magnetron sources so far. Furthermore those novel microwave source might be useful for microwave sustained plasma generators for plasma activation of CO_2 in the frame of next Helmholtz Research Program “Materials and Technology for the Energy Transition”. Therefore the novel lab for plasma chemistry using atmospheric microwave plasma has been upgraded with novel plasma diagnostics. The status of major projects is briefly introduced in the following chapters.

4.1 Plasma Chemistry

Contact: Dr. Sergey Soldatov

The plasma sustained with short microwave pulses is a promising approach since it enables independent control of mean and peak microwave power supplied to the plasma. This helps to establish non-equilibrium plasma states which is unique at atmospheric pressure. Moreover it enables the control of gas temperature that might be useful for future reactors combined with catalyst and oxygen separation membranes. To improve the understanding of mechanisms of energy transfer and equilibration between rotational and vibrational molecular states as well as between electrons and heavier plasma particles, the Optical Emission Spectroscopy (OES) with nanosecond time resolution is employed. In 2019 is was used to follow the evolution of vibrational and rotational temperatures within a single microwave pulse (see Fig. 4.1.1) and to prove non-equilibrium states in atmospheric plasma. For that purpose, the intensified CCD camera is synchronized with a solid state microwave generator (Fig. 4.1.1) thus enabling acquisition of OES spectra at well-defined time windows with respect to pulse start. Systematic studies on correlation of CO_2 conversion efficiency and pulse parameters as well as gas flow have confirmed the advantage of the pulsed energy approach as compared to continuous energy supply. The characterization of pulsed microwave plasmas requires the knowledge of many plasma parameters. One of most important is the density of electrons. Therefore we have considered microwave reflectometry/interferometry as an alternative approach. It was developed and used for the measurement of plasma densities in a surfaguide plasma torch at atmospheric pressure where the main elements of the system are shown in Fig. 4.1.2.

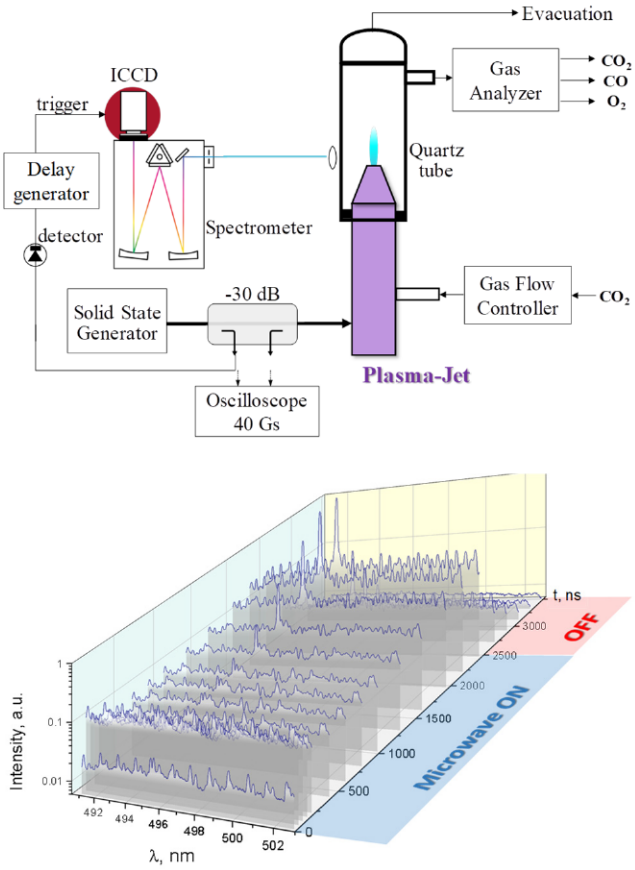

Fig. 4.1.1: Scheme of ns-resolution OES, synchronized with pulsed microwave source (top). Emitted plasma light spectra versus time (bottom).

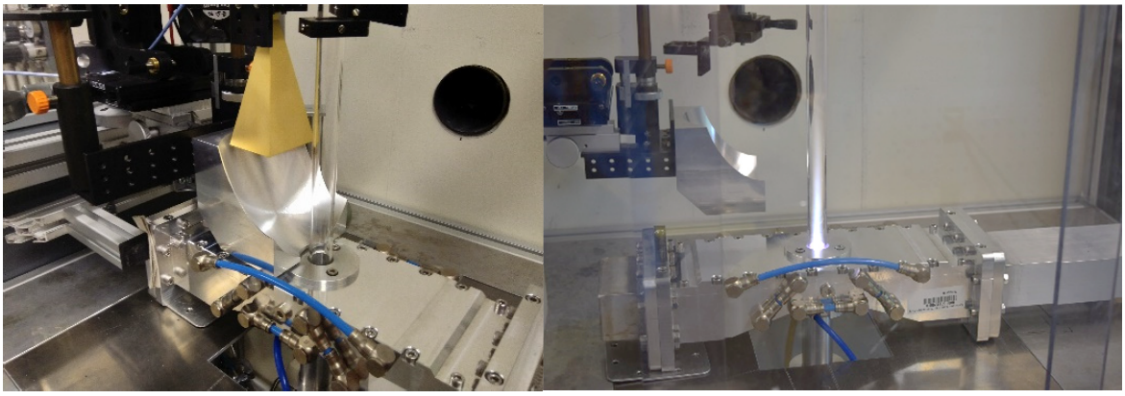

Fig. 4.1.2: Microwave reflectometer for surfaguide plasma experiment.

4.2 e-KOMFORT

Contact: M.Sc. Vasileios Ramopoulos

Comfort is increasingly a decision criterion for buying a car. High quality materials and comfort are the interface to the user. Today, cars are fitted with up to 9 m^2 of technical textiles, which make the car more attractive in terms of look and feel. Such decorative materials have to be laminated by very energy and time-consuming processes. Suitable microwave technology and suitable adhesives allow a direct and selective heating and activation of the adhesive. This leads to significant energy savings of more than 70% and to higher productivity. Accordingly, the aim of the project is to develop an optimized microwave process to support the lamination of the pre-coated and prefixed textile to the substrate.

However, a successful microwave heating of the coating-adhesive-substrate sandwich structure requires the detailed knowledge of the dielectric properties of the materials used. Therefore, an appropriate measurements setup was developed that enables the characterization of sandwich structures. This system is based on a split cylindrical resonator (see Fig. 4.2.1 (left)). The cavity design allows the excitation of the TE_{111}-mode at 2.45 GHz and provides an unloaded Q-factor of about 12000. Furthermore a full-wave 3D electromagnetic model of the experimental setup was developed to separate the permittivity of the adhesive when measuring the textile coated with it.

Based on the measured dielectric properties a suitable microwave tool and microwave applicator were designed (see Fig. 4.2.1 (right)). This microwave applicator has a hexagonal cross section with 1 m in diameter and 1 m in length and cut in the horizontal plane of symmetry. The microwave power generated by solid state amplifiers will be fed into the applicator by space and cost efficient loop antennas. According to actual simulation results, no significant deterioration of the field uniformity in the microwave chamber is expected from the new antenna concept. The antenna positioning and orientation was chosen to ensure the lowest possible cross coupling among the antennas and at the same time to allow the efficient excitation of as many field structures (modes) as possible.

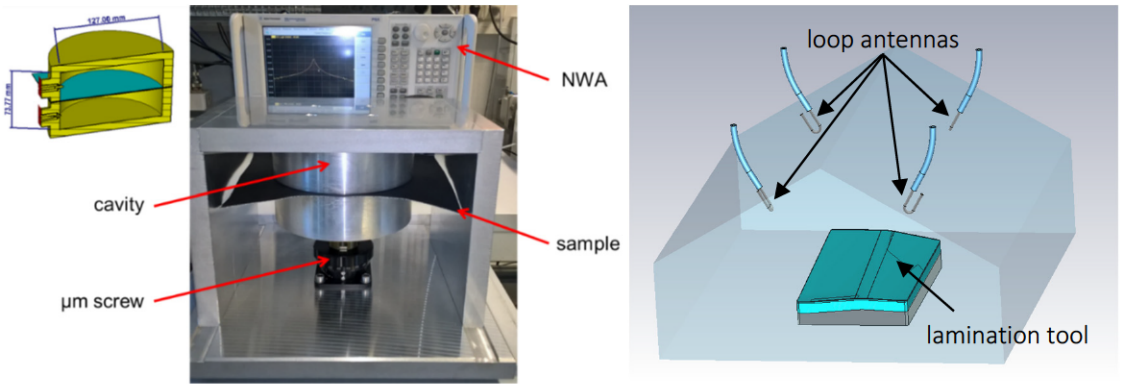

Fig. 4.2.1: Dielectric measurements setup (left); Designed microwave applicator (right).

Funding: 6th Energy Research Programme of the Federal Government of Germany, support code 03ET1576A

4.3 High power solid-state microwave generators

Contact: M.Sc. Dominik Neumaier

Microwave heating offers several advantages compared to conventional heating methods. The major advantages are the volumetric heating effect and the selective heating feature. Therefore, the microwave heating can significantly improve cycle time and energy efficiency of several heating processes. A main challenge of dielectric heating in an industrial scale is to achieve a homogenous temperature distribution in the product, because of the standing waves inside a microwave cavity. The aim of this project is to develop a novel high power solid-state generator (1 kW, 2.4 GHz to 2.5 GHz) in cooperation with the company HBH Microwave GmbH (HBH) and demonstrate its advantages in homogenous microwave heating compared to classical magnetron oscillators. A solid state amplifier offers the opportunity to do a precise control in amplitude, phase and frequency in a very fast manner (1 ms). In Addition, this high power microwave generator also allows creating very short pulses (minimum pulse length: 10 ns), which can be beneficial in microwave sustained plasma applications (see chapter 4.1).

A measurement setup was built up and improved for demonstrating the advantages of this new technology. For testing purpose, a cavity (535 mm x 510 mm x 395 mm) was designed with up to six antennas but only one antenna is used at the same time till now. The microwave power generator can directly measure the frequency-dependent forward and reflected power and therefore allows detecting the resonance frequencies of the eigenmodes of the cavity including a flat load. By using the infrared camera the heating pattern of each eigenmode can be presented (see Fig. 4.3.1). An optimization algorithm taking into account all excitable eigenmodes (about 30) allows improving heating uniformity significantly (see Fig. 4.3.1).

In 2019 an industrial scale hexagonal cavity (diameter of the circumcircle: 1050 mm, depth 1050 mm) has been build, waiting for the delivery of six 1 kW solid-state microwave generators in 2020.

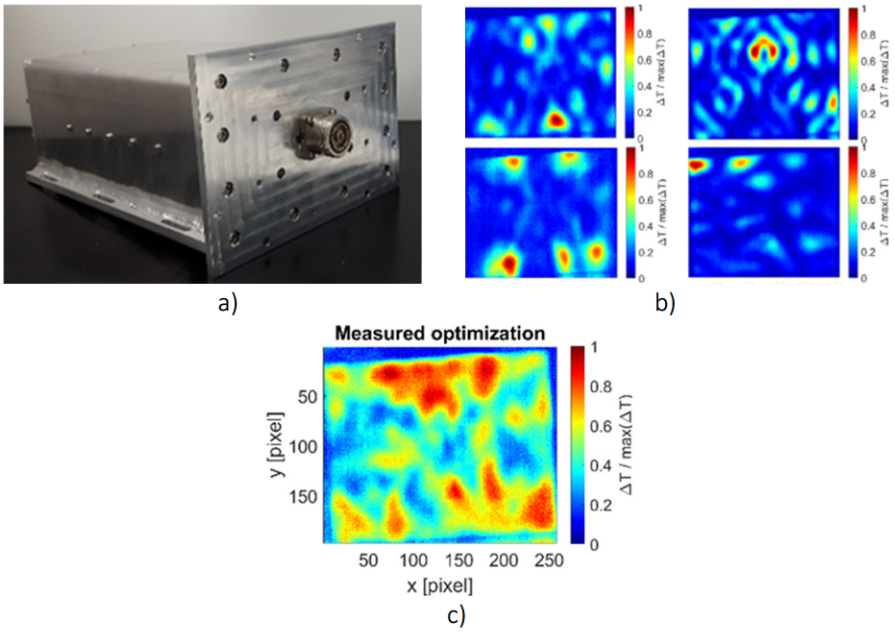

Fig. 4.3.1: Prototype of a 500 W solid state microwave source (a) and a comparison of measured single eigenmodes (b) and an optimized superposition of several eigenmodes (c).

Funding: ZIM cooperation project, support code ZF4204602PR

4.4 Energy-efficient production of robust carbon fibers (REINFORCE)

Contact: M.Sc. Julia Hofele

Carbon fibers are widely used in lightweight applications, but the carbon fiber production is rather expensive and energy intensive compared to the production of aluminum and steel. Microwave heating has the benefit of heating in the volume and thus may lead to faster heating rates. For this reason, the goal of the project is to research the production of carbon fibers with dielectric heating.

The measurement set up, seen in Fig. 4.4.1, was built and it was possible for the first time to track the temperature dependence of the dielectric properties during the stabilization reaction. As it can be evaluated from Fig. 4.4.2 the dielectric properties are strongly temperature dependent and the reaction progress can be tracked during the isothermal holding time. Based on those results a new cavity was designed in order to heat the fiber with microwaves. The next steps will be to put the new cavity into operation, to evaluate the reactions kinetics and to determine the stability criteria for the microwave process.

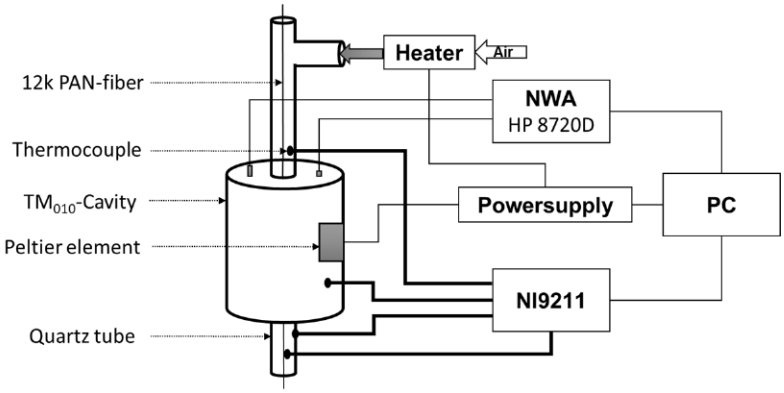

Fig. 4.4.1: Schematic of the set up for conventional heating and measurement of the dielectric properties.

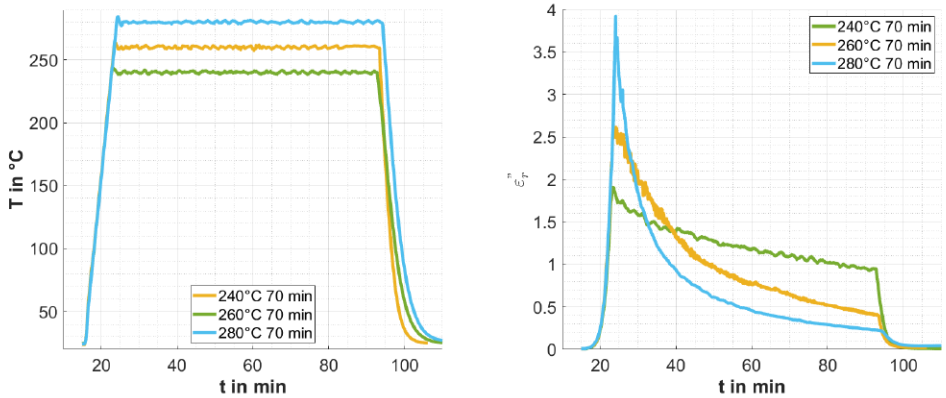

Fig. 4.4.2: Results of the temperature dependent dielectric loss measurements for PAN fibers. (left) Applied heating profile versus time. (right) Comparison of the dielectric loss change versus time for different finale temperatures and a constant holding time of 70 min.

Funding: ZIM cooperation project; support code ZF4204603SY7

4.5 Smart tomographic sensors for advanced industrial process control (TOMOCON)

Contact: M.Sc. Adel Omrani Hamzekalaei

The European Marie Skłodowska-Curie Training Network "Smart tomographic sensors for advanced industrial process control (TOMOCON)" joins 12 international academic institutions and 15 industry partners, who work together in the emerging field of industrial process control using smart tomographic sensors. The network shall lay the scientific and technological fundamentals of integrating imaging sensors into industrial processes and will demonstrate its functional feasibility on lab and pilot-scale applications.

4 doctoral researchers at 3 European academic institutes (Chalmers University of Technology, University of Eastern Finland and KIT), are engaged in the development of microwave and electrical capacitance tomography (MWT and ECT), respectively and its application in microwave drying of porous materials. Those are applied to detect the moisture distribution in a porous material and to provide information to get a feedback for the process control. The technology finally is planned to be demonstrated on an industrial scale conveyor belt system for microwave assisted drying of polymer foams. In a first approach a virtual demonstration based on Simulink software has been developed, including process simulation, forward and inverse problem solvers for the ECT and MWT tomographic sensors as well as algorithms for process control.

During the drying process of polymer foam, the problem of non-uniform heating and drying has to be solved by optimized control of the microwave power distribution, which will allow time and energy saving in the process. Such a precise microwave power control requires non-invasive in-situ measurement of the unknown distribution of moisture inside the material. Thus, microwave tomography and electrical capacitance tomography sensors will be developed and installed to estimate the moisture distribution inside the foam. This information will further be used by the controller to achieve a maximum efficiency.

A first approach of microwave tomography measurement set-up is illustrated in Fig. 4.5.1 (left). X-band (8.2-12.4 GHz) horn antennas are used for transmitting/receiving the electromagnetic signals. This kind of antenna is chosen to avoid electromagnetic interferences with 2.45 GHz from the high power microwave oven. The reflected electromagnetic waves from the foam with the cross-section of 50 cm x 7.6 cm are measured with a vector network analyzer (VNA) and stored in a matrix. The different scattered fields corresponding to the various moisture levels are depicted in Fig. 4.5.1 (Right).

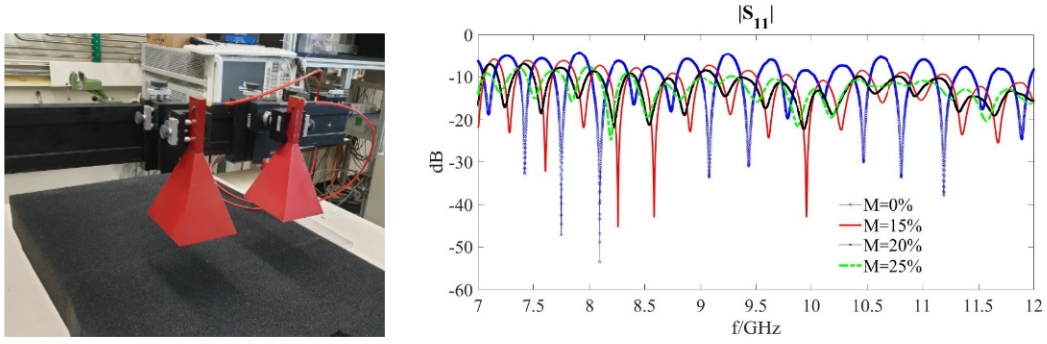

Fig. 4.5.1: (Left) Microwave tomography measurement set-up (Right) Return loss corresponding to different moisture levels.

Funding: H2020-MSCA-ITN-2017; Grant agreement 764902; www.tomocon.eu

4.6 Innovative microwave pultrusion for the cycle controlled sequential curing of fiber reinforced plastics for modular automated manufacture of complex components (IMPULS)

Contact: M.Sc. Moritz Engler

Pultrusion is a manufacturing process for the continuous production of fiber-reinforced polymer profiles, where reinforcing fibers are impregnated with a thermoset resin and then pulled though a heated die, which forces the material into the desired cross section and simultaneously cures the resin. Due to the continuous nature of the process it is significantly more economical than other manufacturing methods for fiber-reinforced composites. However the nature of the process limits it to constant cross section profiles which are straight or of constant radius.

The IMPULS Project aims to develop a microwave powered pultrusion process for the production of carbon fibre-reinforced composite profiles. The advantage of microwave heating compared to the conventional heating process lies in the instantaneous volumetric heating of the structure, which allows curing of the resin without heating the shape defining dice. By switching off the microwave power source, the curing reaction can therefore be interrupted instantaneously, thus allowing the creation of uncured intermediate sections. These sections can then be reprofiled or bent to a desired shape in a following production step. When the microwave is switched off the material currently inside the heating zone will end up in an undefined intermediate curing stage. For the process to be useful these intermediate sections need to be well defined and as short as possible. This introduces two of the main challenges of the microwave applicator design. First, limiting the heating zone to the shortest possible length, which at the operating frequency of 2.45 GHz means focusing of the electric field to a fraction of the wavelength. And second, the thermal management of the tool, to avoid indirect heating of the tool without cooling the profile too much to prevent proper curing of the resin. A variety of applicator concepts has been developed. A first design has already been used for first trials, while a second more advanced applicator is currently in the final design stages.

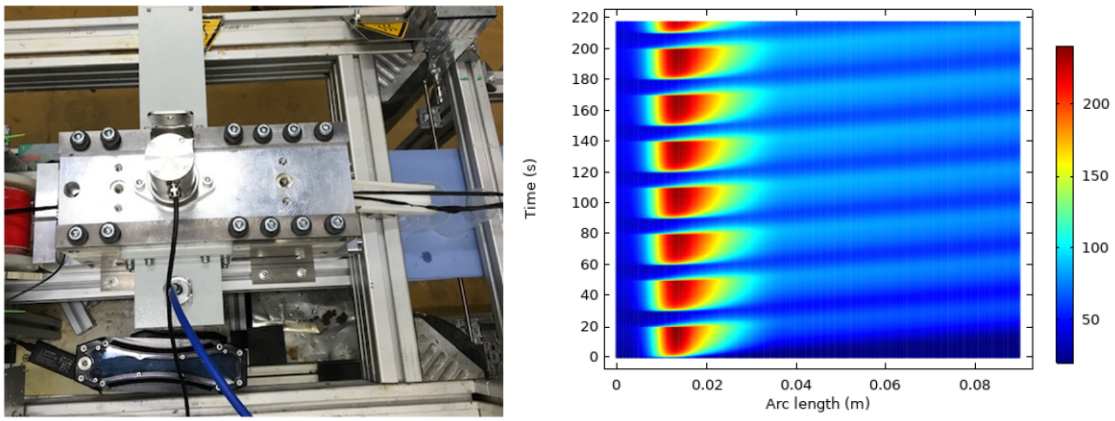

Fig. 4.6.1: Left: Microwave applicator during pultrusion; Right: Simulated temperature at the profile center as a function of position and time.

Funding: BMWi, ZIM Kooperationsprojekt, support code: ZF4204604BL8

4.7 3D Microwave Printing of Composites

Contact: Dr. Nanya Li

Continuous carbon fibers show great promise as reinforcement materials to improve the stiffness, strength to weight ration and designability of 3D printed polymer parts, or known as additive manufacturing. Current 3D printing processes of continuous carbon fiber reinforced thermoplastic (CFRTP) composites lack of abilities to manufacture parts with fast speed and energy efficiency. The challenges are caused by the slow and contact needed heat transfer from the heating nozzle to the CFRTP filament. Microwaves (frequencies between 300MHz and 300GHz) can penetrate composite materials without contact and provide the benefits of selective, volumetric and energy efficient heating. The selective and volumetric heating allows the rapid and uniform heating of even large-diameter CFRTP filaments. In this project, the 3D microwave printing technology is presented to fabricate continuous carbon fiber reinforced composites with faster speed and less energy consumption.

In this project, we invented the first 3D microwave printer (3DMP) to manufacture the continuous carbon fiber reinforced polymer composites and applied a patent. An ingenious microwave applicator by taking the carbon fibers as a perfect microwave absorbing material was designed and manufactured. The printing path planning method was developed for the 3DMP of continuous carbon fiber reinforced composites. Under required load conditions, the stress transmission paths inside the composites were calculated and converted to the printing path of the continuous carbon fiber reinforced filament. A prototype system with 10 times faster printing speed than conventional printing was already demonstrated successfully. This disruptive technology is clearly the answer to the next-generation lightweight carbon fiber reinforced composites.

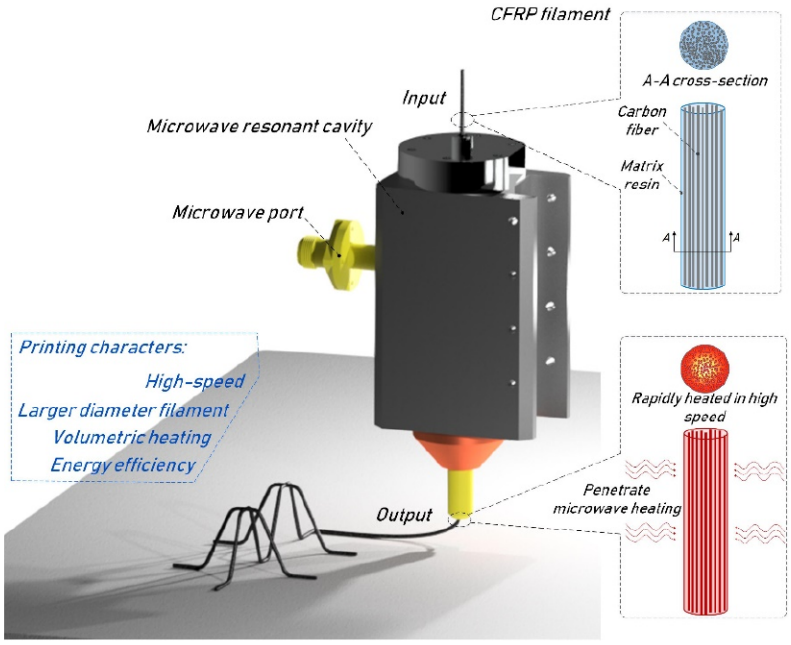

Figure. 4.8: 3D microwave printing technology of continuous carbon fiber reinforced composites.

Funding: Alexander von Humboldt Research Project, German Federal Ministry for Education and Research

Involved Staff

M. Engler, Frau J. Hofele, Prof. J. Jelonnek, Dr. N. Li, **Dr. G. Link**, D. Neumaier, V. Nuss, Adel Omrani, V. Ramopoulos, T. Seitz, S. Soldatov, Frau S. Wadle

Journal Publications

Brovko, A.; Link, G. (2019). Numerical Study of Eigenmodes Propagation Through Rectangular Waveguide with Quarter-Wave Chokes on the Walls. Recent Research in Control Engineering and Decision Making. Ed.: O. Dolinina, 162–172, Springer Fachmedien Wiesbaden, Wiesbaden.

Li, N.; Link, G.; Wang, T.; Ramopoulos, V.; Neumaier, D.; Hofele, J.; Walter, M.; Jelonnek, J. (2019). Path-designed 3D printing for topological optimized continuous carbon fibre reinforced composite structures [in press]. Composites / B, Article no: 107612.

Li, Y.; Li, N.; Zhou, J.; Cheng, Q. (2019). Microwave curing of multidirectional carbon fiber reinforced polymer composites. Composite Structures, 212, 83–93.

Appendix

Equipment, Teaching Activities and Staff

IHM is equipped with a workstation cluster and a large number of experimental installations: KEA, KEA-ZAR, three GESA machines, eight COSTA devices, one abrasion and one erosion teststand, two gyrotron test facilities with one common power supply and microwave-tight measurement chamber, one compact technology gyrotron (30 GHz, 15 kW, continuous wave (CW)), several 2.45 GHz applicators of the HEPHAISTOS series, one 0,915 GHz, 60 kW magnetron system, one 5.8 GHz, 3 kW klystron installation and a low power microwave laboratory with several vectorial network analysers.

The project FULGOR, targeting for a renewal of the KIT gyrotron teststand is progressing. In 2013, an agreement on the project structure including the involvement of the KIT project and quality management has been achieved. The final start of the procurement of the equipment was in 2014.

Prof. John Jelonnek has continued to teach the lecture course entitled “High Power Microwave Technologies (Hochleistungsmikrowellentechnik)” for Master students at KIT. Prof. Georg Müller has continued to teach the lecture on “Pulsed Power Technologies and Applications” at KIT. Dr. Gerd Gantenbein has been teaching the part “heating and current drive” of the lecture “Fusionstechnologie B” by Prof. R. Stieglitz, IFRT. Dr.-Ing. Martin Sack hold the lecture course “Elektronische Systeme und EMV” at KIT.

At the turn of the year 2019/2020 the total staff with regular positions amounted to 40 (20 academic staff members, 10 engineers and 10 technical staff member and others).

In addition 19 academic staff members, 2 engineer and 5 technical staff members (and others) were financed by acquired third party budget.

In course of 2019, 2 guest scientists, 12 PhD students (1 of KIT-Campus South, 11 of KIT-Campus North, 1 Scholarship, 1 in cooperation with IPP Greifswald), 2 DHBW student, 3 trainees in the mechanical and electronics workshops worked in the IHM. 5 Master students have been hosted at IHM and 3 Bachelor student has been at IHM during 2019.

Strategical Events, Scientific Honors and Awards

M.Sc. Tobias Ruess received the “Best Poster Award at the 20th International Vacuum Electronics Conference (IVEC)”, Busan (South Korea).

M.Sc. Vaileios Ramopoulos received the “Best Oral Presentation Award” at the 53rd Microwave Power Symposium (IMPI 53) in Las Vegas, Nevada, USA.

Dr. Sahar Akaberi received the “1st Award young researcher competition” at the 3rd World Congress on Electroporation Pulsed Electric Fields in Biology, Medicine Food and Environmental Technologies, in Toulouse, France.

M.Sc. Damaris Krust received the “Students Poster Award”, beim 3rd World Congress on Electroporation Pulsed Electric Fields in Biology, Medicine Food and Environmental Technologies, in Toulouse, France.

M.Sc. Dominik Neumaier received the “Best Student Paper Award“ at the der 17th International Conference on Microwave and High Frequency Heating (AMPERE) in Valencia, Spain.

Longlasting Co-operations with Industries, Universities and Research Institutes

- Basics of the interaction between electrical fields and cells (Bioelectrics) in the frame of the International Bioelectrics Consortium with Old Dominion University Norfolk, USA; Kumamoto University, Japan; University of Missouri Columbia, USA; Institute Gustave-Roussy and University of Paris XI, Villejuif, France; University of Toulouse, Toulouse, France, Leibniz Institute for Plasma Science and Technology, Greifswald, Germany.
- Desinfection of hospital wastewater by pulsed electric field treatment in cooperation with University of Mainz and Eisenmann AG.
- Integration of the electroporation process for sugar production with SÜDZUCKER AG.
- Development of protection against corrosion in liquid metal cooled reactor systems in the following EU-Projectes: LEADER, GETMAT, MATTER, SEARCH (Partner: CEA, ENEA, SCK-CEN, CIEMAT).
- Development of large area pulsed electron beam devices in collaboration with the Efremov Institute, St. Petersburg, Russia.
- Experiments on liquid Pb and PbBi-cooling of reactor systems with the Institute for Physics and Power Engineering (IPPE), Obninsk, Russia.
- Development, installation and test of the complete 10 MW, 140 GHz ECRH Systems for continuous wave operation at the stellarator Wendelstein W7-X in collaboration with the Max-Planck-Institute for Plasmaphysics (IPP) Greifswald and the Institute of Interfacial Process Engineering and Plasma Technology (Institut für Grenzflächenverfahrenstechnik und Plasmatechnologie, IGVP) of the University of Stuttgart.
- Development of the European ITER Gyrotrons in the frame of the European GYrotron Consortium (EGYC) and coordinated by Fusion for Energy (F4E). The other members of the Consortium are CRPP, EPFL Lausanne, Switzerland, CNR Milano, Italy, ENEA, Frascati, Italy, HELLAS-Assoc. EURATOM (NTUA/NKUA Athens), Greece. The industrial partner is the microwave tube company Thales Electron Devices (TED) in Paris, France.
- Development of new diagnostic systems for improvement of electron guns for gyrotrons and cavity interaction calculations in collaboration with the St. Petersburg Polytechical University, Russia and the University of Latvia, Latvia.
- Development of Microwave Systems of the HEPHAISTOS Series for materials processing with microwaves with the Company Vötsch Industrietechnik GmbH, Reiskirchen.